Regularization errors introduced by the one-fluid formulation in the solution of two-phase elliptic problems

Daniel Fuster, Yassine Mimoh

Highlights

Regularization errors introduced by the one-fluid formulation in the solution of two-phase elliptic problems

Daniel Fuster, Yassine Mimoh

- Formulation of the problem of the error estimation introduced by the regularization of fluid properties on the solution of elliptic equations for multiphase flow problems.
- Derivation of a first order model for the estimation of regularization errors.
- Analysis of the structure of regularization errors using analytical examples.
- Investigation of the relevance of regularization errors in numerical solutions of the Laplace/Poisson equation for problems in the presence of two phases.

Regularization errors introduced by the one-fluid formulation in the solution of two-phase elliptic problems

Daniel Fuster[a,*], Yassine Mimoh[a]

[a]*Sorbonne Université, Centre National de la Recherche Scientifique, UMR 7190, Institut Jean Le Rond D'Alembert, F-75005 Paris, France*

Abstract

This manuscript discusses the structure of the errors in the solution of elliptic problems introduced by the regularization of the fluid properties discontinuity in a small region of finite size. By using a multiscale approach, the problem of the error calculation is splitted into an outer problem, where the regularization region is replaced by a sharp interface, and an inner local one dimensional problem that eventually imposes effective jump conditions across the interface for the outer problem. Except in some particular cases, the use of regularization techniques introduces first order errors in the solution imposing an error flux jump that is proportional to the tangential Laplacian of the averaged solution and an error jump that is proportional to the normal flux, both multiplied by a prefactor that depends on the averaging rule used. In general, the optimal averaging procedure is shown to depend on the structure of the problem at hand. The errors introduced by standard arithmetic and harmonic averages are obtained for various analytical and numerical examples which are used to discuss the nature of the errors introduced and the importance of first order errors in the solution. The influence of the ratio between the regularization thickness and the grid size is also investigated in numerical implementations of the one-fluid model.

Keywords: multiphase systems, one-fluid model, regularization techniques, error estimation

1. Introduction

The development of numerical methods for the simulation of complex multiphase flows is a topic of intense research due to the large amount of industrial and enviromental applications involved. This open research field faces different challenges when trying to numerically capture the influence of discontinuities

*Corresponding author:
Email address: fuster@dalembert.upmc.fr (Daniel Fuster)

on the structure of the solution. One method to account for the influence of fluid properties discontinuities on the solution is to introduce effective averaged quantities. This strategy has attracted the attention of many researchers with different objectives. For periodic systems, homogeneization techniques allow to define effective fluid properties that model the acoustic response of multiphase systems theoretically [5, 18, 37] and also numerically [2, 29]. In the context of solid mechanics, homogeneization techniques are also very popular to model the response of systems with inclusions [15]. Some other local homogeneization approaches for diluted bubbly systems have been proven both to reproduce well the influence of individual bubbles on a liquid and to predict the averaged response of bubble screens [21] and bubble clusters [9].

The use of averaged methods to replace the existence of discontinuities also finds application in communities developping Direct Numerical Simulation techniques for multiphase flow problems. Due to the difficulties to treat the appearance of discontinuities in multidimensional numerical methods, some regularization methods have become very popular in order to replace the discontinuity by a rapidly varying function over a few number of cells. Regularization techniques are typically justified invoking either local volume averaging, time averaging, or classical statistical averaging principles based on ergodicity theories [8]. Although some approaches propose to use modified equations in the regularization region [6, 17], many approaches simply consist in replacing the discontinuous coefficients by a given averaging rule and a smoothing function. Due to their simplicity and robustness, methods based on the advection of a Level Set function or the fraction of a reference fluid have been extensively developed by scientific and industrial communities and implemented in commercial and open-source scientific CFD codes that are nowadays extensively used for a wide spectrum of applications (see [4, 22, 23, 28, 35, 36] just to mention a few). These methods resort to the definition of effective properties in a thin region around the actual interface position introducing localized sources to capture the jump of primitive variables and their flux across and interface when present. For example, the Volume of fluid method (VOF) is typically associated to the one-fluid approach [24, 32] (also known as whole-fluid approach [26]) to solve the Navier-Stokes equations introducing averaged properties and localized sources that only regularize the discontinuity between cells neighbouring the predicted interface location, being possible to find also methods regularizing the solution in larger stencils [34]. Other families of methods based on the Level Set function [3, 30], typically smear the variations in a region that occupies several cells. These methods have been shown to provide accurate results for problems involving heat transfer problems [19], electrodydrodynamics [31] and compressible multiphase flows [10, 25, 27] among many other examples. However, despite the wide use of these family of methods by CFD communities, there is still an open debate about the correct choice of the averaging procedure [11, 14] and the convenience to introduce correction terms at the interface. Although theoretical arguments are usually given to defend a particular choice, usually the lack of a systematic discussion about the errors introduced by the method and averaging

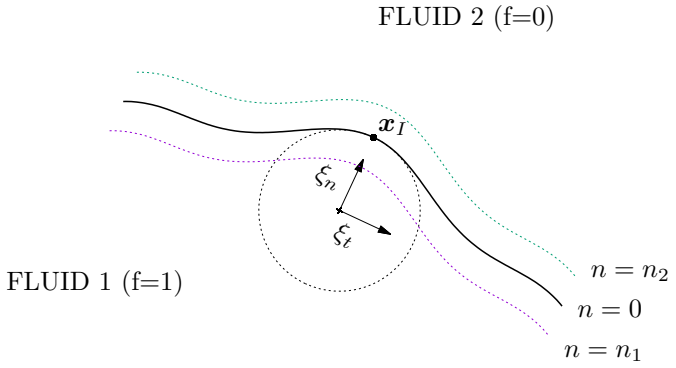

Figure 1: Schematic view for a two-dimensional problem of the different definitions used for the analysis of the errors generated by the regularization of the diffusion coefficients into a region of thickness Δ.

rule chosen to regularize the interface prevents quantifying the impact of a given choice for a particular problem. For instance, it is known that the harmonic mean provides exact results for the solution of one-dimensional elliptic equations [32], but a rigorous and detailed analysis of the errors introduced with this type of approaches in a general case are less common. Understanding the error introduced by the regularization approach is important for the optimal choice of the averaging proceduces [31], the development of efficient adaptive mesh refinement strategies capable to reduce the error present in the solution [1, 7, 13, 33] and the development of more accurate methods capable to compensate for the errors introduced in the solution when regularizing the coefficients [12]. In this work we propose to take a step forward in this direction and to push forward a model able to capture the errors introduced by any given averaged procedure to represent the influence of a sharp interface for the solution of elliptic problems.

The manuscript is structured as follows. The general problem is presented in Section 2, while the equations representing the regularization errors are presented in Section 3. Section 4 presents first order solutions for flat interfaces before discussing the effect of curvature in Section 5. In Section 6, various problems with analytical solutions for both the discontinuous and regularized problem are used to asses the correctness and accuracy of the first order models. Finally we discuss the relevance of these regularization errors in numerical solutions as a function of the ratio between the grid size and the regularization thickness before the conclusions and perspectives are presented.

2. Problem setup

In this work we consider the problem of a Poisson equation with discontinuous coefficients

$$\nabla \cdot (D_i \nabla \phi_i) = s_i, \tag{1}$$

with i=1,2 and null jump conditions on the field variables and the flux across the interface

$$[[\phi]] = 0, \quad [[D\nabla\phi \cdot \boldsymbol{n}]] = 0, \quad \boldsymbol{x} = \boldsymbol{x}_I$$

where $\boldsymbol{n}$ is the normal to the interface located at $\boldsymbol{x}_I$ and the jump is defined as $[[\phi]] = \phi_2 - \phi_1$.

We want to evaluate the error of any averaged procedure based on the definition of averaged quantities such that the ODE to be solved becomes

$$\nabla \cdot (\tilde{D} \nabla \tilde{\phi}) = \tilde{s}, \tag{2}$$

where $\tilde{D}$ is an arbitrary continuous coefficient that varies $[[D]]$ over a characteristic small distance Δ which spatial structure depends on a regularization function $f(n)$ bounded between 0 and 1 (see figure 1). The regularization function depends on the signed distance function n and it is assumed to only vary in a compact and narrow region with a thickness $n_2 - n_1$ around the exact position of a sharp interface. The value of Δ is defined as the characteristic length in which the coefficients vary significantly so that although the model allows setting independently the values of n_1, n_2 and Δ, it will be convenient for practical purposes to approximate $n_1 \approx -\Delta/2$ and $n_2 \approx \Delta/2$ irrespective of the thickness of the actual region where f varies. This may be important in order to extend the results of these analyses to methods based on the introduction of hyperbolic tangent or other regularization functions with no compact support [35]. In this work, we will particularize some of the general expressions found to the case where errors are introduced by a linear variation of the phase field

$$f = \begin{cases} 1, & n < n_1 \\ 0.5 - \frac{n}{\Delta}, & n_1 \leq n \leq n_2 \\ 0, & n > n_2 \end{cases} \tag{3}$$

with $n_1 = -\Delta/2$ and $n_2 = \Delta/2$.

3. General error equation

The equation describing the error introduced by the regularization of the discontinuous coefficients

$$\epsilon_i = \phi_i - \tilde{\phi},$$

can be obtained by subtracting eq. 1 from eq. 2

$$\nabla \cdot (D_i \nabla \epsilon_i) = S_{\epsilon_i}, \tag{4}$$

where S_ϵ is a source of error localized in the region of space where the coefficients have been regularized and expressed as a function of the regularized solution $\tilde{\phi}$

$$S_{\epsilon_i} \equiv \nabla \cdot ((\tilde{D} - D_i)\nabla\tilde{\phi}) + s_i - \tilde{s}. \tag{5}$$

Note that the error is subdivided into two regions where by convention $i = 1$ applies to the region $n \leq 0$ while $i = 2$ applies to $n \geq 0$.

Jump conditions need to be specified to solve equation 4. It is straightforward to see that the error is continuous everywhere in the domain including the surface defined by the exact position of the interface $\boldsymbol{x}_I$,

$$[[\epsilon]] = 0 \quad \boldsymbol{x} = \boldsymbol{x}_I. \tag{6}$$

The normal flux is continous everywhere except at the position of the exact interface position, where the definition of the error imposes

$$D_1\frac{\partial\epsilon_1}{\partial n} = D_1\frac{\partial\phi_1}{\partial n} - D_1\frac{\partial\tilde{\phi}}{\partial n}, \quad \boldsymbol{x} = \boldsymbol{x}_I,$$
$$D_2\frac{\partial\epsilon_2}{\partial n} = D_2\frac{\partial\phi_2}{\partial n} - D_2\frac{\partial\tilde{\phi}}{\partial n}, \quad \boldsymbol{x} = \boldsymbol{x}_I.$$

Subtracting both expressions and imposing the continuity of fluxes in the sharp approach we finally obtain that the jump condition of the error flux at n=0 can be expressed as a function of $\tilde{\phi}$ as

$$[[D\frac{\partial\epsilon}{\partial n}]] = -[[D]]\frac{\partial\tilde{\phi}}{\partial n}, \quad \boldsymbol{x} = \boldsymbol{x}_I. \tag{7}$$

Equation 4 with the jump conditions 6-7 and null Dirichlet boundary conditions across the domain limits allow us to obtain the error introduced by the regularization of a sharp interface by the introduction of a smooth transition region.

In the limit of a thin regularization region compared to the large scale L_0 associated with the problem at hand (e.g. $\Delta/L_0 \to 0$) we separate the problem into an outer region including the bulk regions defined by f=1 and f=0, and the inner problem where the local error $\tilde{\epsilon}$ is defined inside the regularized region with the associated lengthscale Δ.

The inner problem can be written locally for point $\boldsymbol{x}_I$ using generalized orthogonal coordinates where a local curvilinear coordinate system $(\xi_n, \xi_{t_1}, \xi_{t_2})$ is defined such that ξ_n is normal to the isolines of $\tilde{D}$ and ξ_{t_1} and ξ_{t_2} denote two tangential orthogonal directions. The resulting Poisson equation (equation 4)

$$\frac{1}{h_{\xi_{t_1}}h_{\xi_{t_2}}h_{\xi_n}}\frac{\partial}{\partial\xi_n}\left(\frac{h_{\xi_{t_1}}h_{\xi_{t_2}}}{h_{\xi_n}}D_i\frac{\partial\tilde{\epsilon}_i}{\partial\xi_n}\right) = S_{\epsilon_i} - D_i\mathcal{L}^t(\tilde{\epsilon}_i) \tag{8}$$

needs to be solved with the jump conditions at n=0 (e.g. $\xi_n = \xi_I$) imposed by equations 6-7, where $h_{\xi_{t_1}} h_{\xi_{t_2}} h_{\xi_n}$ represent the metric factors in the local system of coordinates and the tangential Laplacian operator is defined as

$$\mathcal{L}^t(\tilde{\epsilon}) \equiv \nabla \cdot (\nabla\tilde{\epsilon} - (\nabla\tilde{\epsilon} \cdot \mathbf{n})\mathbf{n}).$$

The problem for the outer error ϵ' at kth order is reduced to a pure Laplace equation

$$\nabla \cdot (D_i \nabla \epsilon_i'^{(k)}) = 0, \tag{9}$$

where the interface is replaced by an infinitely thin interface with effective jump conditions to be found by matching the outer and inner solution at the edges of the regularization region

$$\epsilon_1'^{(k)}(n \to 0) = \tilde{\epsilon}_1^{(k)}(n = n_1), \tag{10}$$
$$\epsilon_2'^{(k)}(n \to 0) = \tilde{\epsilon}_2^{(k)}(n = n_2), \tag{11}$$

such that

$$[[\epsilon'^{(k)}]] = \tilde{\epsilon}_2^{(k)}(n = n_2) - \tilde{\epsilon}_1^{(k)}(n = -n_1);$$
$$[[D\nabla\epsilon'^{(k)} \cdot \mathbf{n}]] = D_2(\nabla\tilde{\epsilon}^{(k)} \cdot \mathbf{n})\Big|_{n_2} - D_1(\nabla\tilde{\epsilon}^{(k)} \cdot \mathbf{n})\Big|_{n_1}.$$

This procedure can be followed to derive the error of more complex equations as for example the transient diffusion-reaction equation included in appendix Appendix A (eq. A.4).

In what follows we will derive expressions for the structure of the inner solution and the jump conditions required in the outer problem of steady state solutions. Because the correct treatment of the errors associated to the regularization of the source term are related to the exact structure of it, we restrict ourselves to the discussion of cases where the source term is known ($\tilde{s}_i = s_i$). The analysis of the errors introduced by the regularization of the source is left for future works, although the extension to integrable sources is straightforward.

4. Approximated solutions for flat surfaces

For flat surfaces, we can find the error generated by a flat surface $\epsilon_{f,i}$ rewritting equation 8 as

$$\frac{\partial}{\partial n}\left(D_i \frac{\partial \tilde{\epsilon}_{f,i}}{\partial n}\right) = \frac{\partial}{\partial n}\left((\tilde{D} - D_i)\frac{\partial \tilde{\phi}}{\partial n}\right) + (\tilde{D} - D_i)\mathcal{L}^t(\tilde{\phi}) - D_i\mathcal{L}^t(\tilde{\epsilon}_{f,i}), \tag{12}$$

which can be integrated along the normal direction to obtain a one-dimensional first order differential equation for the structure of the regularization error flux around $\boldsymbol{x}_I$

$$D_i \frac{\partial \tilde{\epsilon}_{f,i}}{\partial n} = (\tilde{D} - D_i)\frac{\partial \tilde{\phi}}{\partial n} + \int_0^n ((\tilde{D} - D_i)\mathcal{L}^t(\tilde{\phi}) - D_i\mathcal{L}^t(\tilde{\epsilon}_{f,i}))dn + c_{f,i}, \tag{13}$$

where, using $\tilde{D}_0$ to denote the averaged coefficient at n=0, the integration constant $c_{f,i}$ is defined as

$$c_{f,i} \equiv D_i \frac{\partial \tilde{\epsilon}_{f,i}}{\partial n}\bigg|_{n=0} - (\tilde{D}_0 - D_i)\frac{\partial \tilde{\phi}}{\partial n}\bigg|_{n=0}. \tag{14}$$

Using the jump condition of the derivative at this point (eq. 7), this constant is readily shown to be equal in both subregions

$$c_f \equiv c_{f,1} = c_{f,2}.$$

The integration of equation 13 leads us to expressions for the error distribution inside the regularization region

$$\begin{aligned} \tilde{\epsilon}_{f,i}(n) &= d_i + n\frac{c_f}{D_i} + \int_0^n \tilde{J}_n \left(\frac{1}{D_i} - \frac{1}{\tilde{D}}\right) dn \\ &+ \int_0^n \left(\int_0^{n'} \left(\frac{\tilde{D}}{D_i} - 1\right) \mathcal{L}^t(\tilde{\phi}) dn\right) dn' - \int_0^n \left(\int_0^{n'} \mathcal{L}^t(\tilde{\epsilon}_i) dn\right) dn' \end{aligned} \tag{15}$$

where $\tilde{J}_n = \tilde{D}\frac{\partial \tilde{\phi}}{\partial n}$ is used to denote the normal flux and d_i is an integration constant that by continuity of the error across $n = 0$ satisfies

$$d_1 = d_2. \tag{16}$$

In the following, we will decompose the error and the variable $\tilde{\phi}$ as

$$\epsilon_i = \epsilon_i^{(0)} + \epsilon_i^{(1)}\Delta + \epsilon_i^{(2)}\Delta^2 + ...$$

$$\tilde{\phi} = \tilde{\phi}^{(0)} + \tilde{\phi}^{(1)}\Delta + \tilde{\phi}^{(2)}\Delta^2 + ...$$

to obtain simplified expressions at a desired order for the error jump conditions of the outer problem and the structure of the inner error.

4.1. Leading order approximation for flat surfaces

The jump conditions for the outer problem can be found at leading order from the evaluation of equations 13-15 at both edges of the regularization region. It is straighforward to see from equation 13 that

$$[[D\frac{\partial \epsilon_f'^{(0)}}{\partial n}]] = 0 \tag{17}$$

provided that

$$\int_{n_1}^0 (\tilde{D} - D_1)\mathcal{L}^t(\tilde{\phi}) dn + \int_0^{n_2} (\tilde{D} - D_2)\mathcal{L}^t(\tilde{\phi}) dn \approx \mathcal{O}(\Delta). \tag{18}$$

To obtain the error jump, we need to obtain the normal flux across the normal direction in the regularization region from the integration of equation 2. When

$$\int_{n_1}^{n_2} (\tilde{s} - \tilde{D}\mathcal{L}_0^t(\tilde{\phi}))dn = \mathcal{O}(\Delta), \tag{19}$$

we readily obtain

$$\frac{\partial \tilde{J}_n}{\partial n} = \tilde{s}(0) - \tilde{D}(0)\mathcal{L}_0^t(\tilde{\phi}^{(0)}) + \mathcal{O}(\Delta). \tag{20}$$

where $\mathcal{L}_0^t(\tilde{\phi}^{(0)})$ denotes the leading order contribution of the tangential Laplacian operator applied to $\tilde{\phi}^{(0)}$ evaluated at $n = 0$. The result is that within the regularization region the normal flux

$$\tilde{J}_n = \tilde{D}\frac{\partial \tilde{\phi}}{\partial n} = \tilde{J}_{n,0}^{(0)} + \mathcal{O}(\Delta), \tag{21}$$

is constant across the normal direction at leading order. With this result and subtracting equation 15 evaluated at the edges of the regularization region we find

$$[[\epsilon_f'^{(0)}]] = 0. \tag{22}$$

provided that

$$\int_{n_1}^{0} \tilde{J}_n \left(\frac{1}{D_1} - \frac{1}{\tilde{D}}\right) dn + \int_{0}^{n_2} \tilde{J}_n \left(\frac{1}{D_2} - \frac{1}{\tilde{D}}\right) dn \approx \mathcal{O}(\Delta). \tag{23}$$

Because the jump conditions across the interface are both zero (eqs. 22-17), when no error is introduced through the domain boundaries the error in both the outer and inner region are both null

$$\tilde{\epsilon}_f^{(0)}(-\Delta/2 \leq n \leq \Delta/2) = \epsilon_f'^{(0)}(\boldsymbol{x}) = 0.$$

It is worth mentioning that conditions 18-19-23 are necessary conditions to obtain convergence for the regularized problem. Although this does not constitute a general proof of convergence for arbitrary definitions of $\tilde{D}$, for non-singular sources and for definitions of the regularized coefficient where $\tilde{D}(\boldsymbol{x}) > 0$, both the normal flux and the tangential Laplacian will be continuous and infinitely differentiable functions implying that the regularized method converges if the definition of $\tilde{D}$ satisfies

$$\int_{n_1}^{n_2} \frac{dn}{\tilde{D}} \approx \mathcal{O}(\Delta), \qquad \int_{n_1}^{n_2} \tilde{D}dn \approx \mathcal{O}(\Delta).$$

We also note that although the normal flux is constant around $\boldsymbol{x}_I$ at leading order, the normal derivative of the regularized solution varies across the regularization zone at the dominant order. Taking advantage from the fact that the flux of the regularized solution converges to that of the sharp problem we can obtain local estimations of the gradients at both sides of the interface as

$$\left.\frac{\partial \phi_1}{\partial n}\right|_{n=0} \approx \frac{\tilde{D}}{D_1}\frac{\partial \tilde{\phi}}{\partial n}, \qquad \left.\frac{\partial \phi_2}{\partial n}\right|_{n=0} \approx \frac{\tilde{D}}{D_2}\frac{\partial \tilde{\phi}}{\partial n}.$$

4.2. First order expressions for flat surfaces

The jump conditions across the interface is approximated at first order from equations 13-15 obtaining

$$\begin{aligned}[[D\frac{\partial \epsilon'_f}{\partial n}]] &= \int_{n_1}^{0}(\tilde{D}-D_1)\mathcal{L}^t(\tilde{\phi})dn + \int_{0}^{n_2}(\tilde{D}-D_2)\mathcal{L}^t(\tilde{\phi})dn + \mathcal{O}(\Delta^2) \\ [[\epsilon'_f]] &= \int_{n_1}^{0}\tilde{J}_n\left(\frac{1}{D_1}-\frac{1}{\tilde{D}}\right)dn + \int_{0}^{n_2}\tilde{J}_n\left(\frac{1}{D_2}-\frac{1}{\tilde{D}}\right)dn + \mathcal{O}(\Delta^2) \quad (24)\end{aligned}$$

As we have seen before, the normal flux and the surface Laplacian is continuous and constant across the regularized region in the normal direction at leading order, thus the expressions for the jump conditions for $\epsilon^{(1)}_{f,i}$ can be written for any definition of the regularization function $f(n)$ as

$$[[D\frac{\partial \epsilon'^{(1)}_f}{\partial n}]] = C_1\mathcal{L}^t_0(\tilde{\phi}^{(0)}) \quad (25)$$

$$[[\epsilon'^{(1)}_f]] = C_2\tilde{J}^{(0)}_{n,0}. \quad (26)$$

When the regularization function can be approximated by eq. 3, the expressions for C_1 and C_2 are

$$C_1 \equiv \int_0^1 \tilde{D}df - \frac{D_1+D_2}{2}, \qquad C_2 \equiv \frac{1}{2}\left(\frac{1}{D_1}+\frac{1}{D_2}\right) - \int_0^1 \frac{df}{\tilde{D}}. \quad (27)$$

It is readily shown that the arithmetic mean

$$\tilde{D} = D_1 f + D_2(1-f)$$

does not introduce any error flux source at the interface at first order at expenses of introducing an error jump

$$[[D\frac{\partial \epsilon'^{(1)}_f}{\partial n}]] = 0, \quad (28)$$

$$[[\epsilon'^{(1)}_f]] = \tilde{J}^{(0)}_{n,0}\left(-\frac{\ln(D_2/D_1)}{[[D]]} + \frac{1}{2}\left(\frac{1}{D_1}+\frac{1}{D_2}\right)\right). \quad (29)$$

On the other hand the use of the harmonic mean

$$\frac{1}{\tilde{D}} = \frac{f}{D_1} + \frac{1-f}{D_2},$$

guarantees the continuity of the error across the interface at expenses of introducing an error flux source that depends on the tangential Laplacian operator applied on the regularized solution

$$[[D\frac{\partial \epsilon'^{(1)}_f}{\partial n}]] = \left(-\frac{D_1+D_2}{2} + \frac{D_1D_2}{[[D]]}\ln\left(\frac{D_2}{D_1}\right)\right)\mathcal{L}^t_0(\tilde{\phi}), \quad (30)$$

$$[[\epsilon'^{(1)}_f]] = 0. \quad (31)$$

The solution of the Laplace problem with the jump conditions above allows obtaining the error field in the bulk regions. Once the error of the outer problem $\epsilon_f^{\prime(1)}$ has been computed, the error inside the regularization region can be obtained at first order from eq. 15 as

$$\tilde{\epsilon}_f^{(1)}(n) = \begin{cases} \epsilon_{f,1}^{\prime(1)}(n \to 0) + \tilde{J}_{n,0}^{(0)} \frac{1}{\Delta} \int_{n_1}^{n} \left(\frac{1}{D_1} - \frac{1}{\tilde{D}} \right) dn, & n_1 \leq n \leq 0, \\ \epsilon_{f,2}^{\prime(1)}(n \to 0) - \tilde{J}_{n,0}^{(0)} \frac{1}{\Delta} \int_{n}^{n_2} \left(\frac{1}{D_2} - \frac{1}{\tilde{D}} \right) dn, & 0 \leq n \leq n_2. \end{cases} \tag{32}$$

Thus, the errors inside the regularization region can be represented as a function of the dimensionless distance n/Δ (directly related to the parameter f), the leading order contribution of the normal flux across the interface (which is constant across the normal direction) and a constant imposed by the solution at point $\boldsymbol{x}_I$ of the outer problem (note that we can use the errors jump condition to eliminate either $\epsilon_{f,1}^{\prime(1)}(n \to 0)$ or $\epsilon_{f,2}^{\prime(1)}(n \to 0)$). One important remark is that the errors inside the diffuse interface region are first order irrespective of the choice of the averaged procedure chosen. In particular for regularization functions satisfying

$$\frac{\partial f}{\partial n} = -\frac{1}{\Delta} + \mathcal{O}(1), \qquad n = 0$$

the local error can be reconstructed from the outer solution when using the arithmetic mean as

$$\tilde{\epsilon}_{f,\text{arith}}^{(1)}(f) = \begin{cases} \epsilon_{f,1}^{\prime(1)}(n \to 0) + \tilde{J}_{n,0}^{(0)} \left(\frac{1-f}{D_1} - \frac{\ln\left(\frac{\tilde{D}}{D_1}\right)}{[[D]]} \right), & 0.5 \leq f \leq 1 \\ \epsilon_{f,2}^{\prime(1)}(n \to 0) - \tilde{J}_{n,0}^{(0)} \left(\frac{f}{D_2} + \frac{\ln\left(\frac{\tilde{D}}{D_2}\right)}{[[D]]} \right), & 0 \leq f \leq 0.5 \end{cases} \tag{33}$$

while for the harmonic mean we find

$$\tilde{\epsilon}_{f,\text{harm}}^{(1)}(f) = \epsilon_{f,1}^{\prime(1)}(n \to 0) + \begin{cases} \tilde{J}_{n,0}^{(0)}(1-f)^2 \frac{[[D]]}{2D_1D_2}, & 0.5 \leq f \leq 1 \\ \tilde{J}_{n,0}^{(0)} f^2 \frac{[[D]]}{2D_1D_2}, & 0 \leq f \leq 0.5. \end{cases} \tag{34}$$

where in this later case we know from eq. 31 that the error jump across the interface of finite thickness is continuous $\epsilon_{f,1}^{\prime(1)}(\boldsymbol{x}_I) = \epsilon_{f,2}^{\prime(1)}(\boldsymbol{x}_I)$. It is worth noting that in the case of the harmonic mean the error difference between the edge of the regularized region and n=0 is symmetric while it is not symmetric in the case of the arithmetic mean, the error jump being significantly larger in the region occupied by the fluid with lower diffusivity.

4.3. Second order expressions for flat surfaces

For completeness, we provide second order accurate expressions of the effective jump conditions introduced by the regularization of the coefficients

$$\begin{aligned}
[[D\frac{\partial \epsilon'_f}{\partial n}]] &= \int_{n_1}^{0} (\tilde{D} - D_1)\mathcal{L}^t(\tilde{\phi})dn + \int_{0}^{n_2} (\tilde{D} - D_2)\mathcal{L}^t(\tilde{\phi})dn \\
&- \Delta D_1 \int_{n_1}^{0} \mathcal{L}^t(\tilde{\epsilon}^{(1)}_{f,1})dn - \Delta D_2 \int_{0}^{n_2} \mathcal{L}^t(\tilde{\epsilon}^{(1)}_{f,2})dn + \mathcal{O}(\Delta^3) \\
[[\epsilon'_f]] &= \frac{\Delta}{2} c_f \left(\frac{1}{D_2} + \frac{1}{D_1}\right) - \int_{0}^{n_2}\int_{n'}^{n_2} \left(\frac{\tilde{D}}{D_2} - 1\right)\mathcal{L}^t(\tilde{\phi})dndn' + \int_{n_1}^{0}\int_{n_1}^{n'} \left(\frac{\tilde{D}}{D_1} - 1\right)\mathcal{L}^t(\tilde{\phi})dndn' \\
&+ \int_{n_1}^{0} \tilde{J}_n \left(\frac{1}{D_1} - \frac{1}{\tilde{D}}\right) dn + \int_{0}^{n_2} \tilde{J}_n \left(\frac{1}{D_2} - \frac{1}{\tilde{D}}\right) dn + \mathcal{O}(\Delta^3)
\end{aligned} \tag{35}$$

where the first order variations of the normal and tangential derivatives across the normal direction need to be accounted for and a first order estimation of the constant c_f is

$$c_f \approx \tilde{J}^{(1)}_{n,0}\Delta = \tilde{J}_{n,0} - \tilde{J}^{(0)}_{n,0}.$$

Note that second order corrections can be obtained subtracting first error expressions from the equations above.

In one-dimensional problems, the harmonic mean leads to null jump conditions when solving the Laplace equation. Indeed this result applies to arbitrary order implying that, consistent with reasonings based on the discretization of the equation [32], harmonic mean provides exact solutions in the bulk regions in 1D. In the case of the arithmetic mean, second order errors introduce an error flux source only for multidimensional problems.

5. Curvature effects

In a general situation the influence of curvature needs to be discussed. For that, the general equation for the inner error (equation 8) is expressed using curvilinear coordinates as

$$\frac{\partial}{\partial n}\left(D_i \frac{\partial \tilde{\epsilon}_i}{\partial n}\right) + \mathcal{K} D_i \frac{\partial \tilde{\epsilon}_i}{\partial n} + D_i \mathcal{L}^t(\tilde{\epsilon}_i) = \frac{\partial}{\partial n}\left((\tilde{D} - D_i)\frac{\partial \tilde{\phi}}{\partial n}\right) + (\tilde{D} - D_i)\mathcal{L}^t(\tilde{\phi}) + \mathcal{K}(\tilde{D} - D_i)\frac{\partial \tilde{\phi}}{\partial n}$$

where the normal derivative is $\frac{\partial}{\partial n} \equiv \frac{1}{h_{\xi_n}}\frac{\partial}{\partial \xi_n}$ and $\mathcal{K}$ is defined as

$$\mathcal{K} \equiv \frac{1}{h_{\xi_n} h_{\xi_{t_1}} h_{\xi_{t_2}}} \frac{\partial}{\partial n}\left(h_{\xi_{t_1}} h_{\xi_{t_2}}\right).$$

For the point $\boldsymbol{x}_I$, the principal curvatures κ_1 and κ_2 allow us to find an approximation of the local orthogonal coordinates by defining a local polar coordinate

system in 2D (Appendix B.1) or an oblate spheroidal coordinate system in 3D (Appendix B.2) for which the isoline of ξ_n at $\boldsymbol{x}_I$, corresponding to the point $(\xi_n, \xi_{t_1}, \xi_{t_2}) = (\xi_I, 0, 0)$, is tangent to the surface. In this local system the local values of the metric factors can be readily computed obtaining that $\mathcal{K} = \kappa_0 + \mathcal{O}(\Delta)$, where κ_0 is the value of the curvature in two-dimensional cases (Appendix B.1), and twice the principal curvature with the smallest absolute value in three dimensional cases (Appendix B.2). Thus, in a general case the presence of curvature introduces an additional error source with respect to a flat surface. For first order estimations of the error and error flux jump conditions required for the outer problem we can use the simplified equation

$$D_i \frac{\partial^2 \tilde{\epsilon}_i}{\partial n^2} + \kappa_0 D_i \frac{\partial \tilde{\epsilon}_i}{\partial n} = \kappa_0 (\tilde{D} - D_i) \frac{\partial \tilde{\phi}}{\partial n} + \frac{\partial}{\partial n} \left((\tilde{D} - D_i) \frac{\partial \tilde{\phi}}{\partial n} \right) + (\tilde{D} - D_i) \mathcal{L}^t(\tilde{\phi}) + \mathcal{O}(\kappa_0 \Delta).$$

The general solution for the normal error flux can be expressed in terms of integrals from the exact location of the interface (e.g. $n = 0$) as

$$D_i \frac{\partial \tilde{\epsilon}_i}{\partial n} = e^{-\kappa_0 n} \left[c_i + \int_0^n \frac{\partial}{\partial n} \left(e^{\kappa_0 n'} (\tilde{D} - D_i) \frac{\partial \tilde{\phi}}{\partial n} \right) dn' + \int_0^n e^{\kappa_0 n'} (\tilde{D} - D_i) \mathcal{L}^t(\tilde{\phi}) dn' \right] + \mathcal{O}(\kappa_0 \Delta^2)$$

which can be simplified for first order error estimations of the normal flux as

$$D_i \frac{\partial \tilde{\epsilon}_i}{\partial n} = c_i (1 - \kappa_0 n) + \left((\tilde{D} - D_i) \frac{\partial \tilde{\phi}}{\partial n} - (1 - \kappa_0 n)(\tilde{D}_0 - D_i) \frac{\partial \tilde{\phi}}{\partial n}\bigg|_{n=0} \right) + \mathcal{L}_0^t(\tilde{\phi}^{(0)}) \int_0^n (\tilde{D} - D_i) dn + \mathcal{O}(\Delta^2)$$

where we recall that $\tilde{D}_0 = \tilde{D}(n = 0)$ and c_i is an integration constant. The structure of the error inside the regularization problem can be obtained at first order from the direct integration of the above expression as

$$\tilde{\epsilon}_i = d_i + \frac{c_i}{D_i} n + \int_0^n \left(\frac{1}{D_i} - \frac{1}{\tilde{D}} \right) \tilde{J}_n dn + \left(\frac{1}{D_i} - \frac{1}{\tilde{D}_0} \right) \tilde{J}_{n,0} + \mathcal{O}(\Delta^2)$$

Imposing the jump conditions to obtain the jump of the integration constants and following the same procedure than before it is easy to show that the jump conditions for the error and normal error flux for the outer problem are zero at leading order, while the expressions at first order remain unchanged with respect to the expressions found for a flat interface

$$[[D \frac{\partial \epsilon'}{\partial n}]] = [[D \frac{\partial \epsilon'_f}{\partial n}]] + \mathcal{O}(\Delta^2),$$

$$[[\epsilon']] = [[\epsilon'_f]] + \mathcal{O}(\Delta^2).$$

Remarkably, curvature does not play any role in first order estimations of the jump conditions for the outer problem, the correction due to the presence of curvature appearing only in the second order estimation of the effective jump conditions required for the resolution of the outer problem and the second order representation of the inner error.

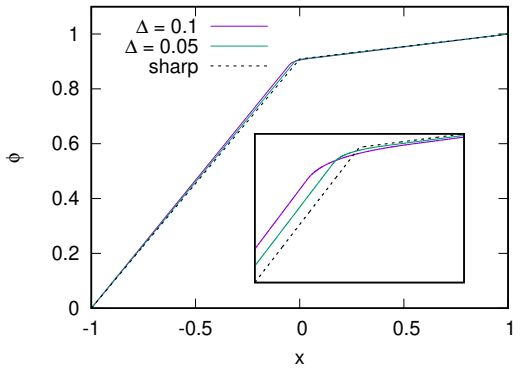

Figure 2: Solution of the 1D Laplace equation for $D_r = 10$ using the arithmetic mean for two different values of the regularization region. With dashed lines we represent the solution of the problem with discontinuous coefficients.

6. Analytical examples

We discuss now the behavior of the error for particular problems where it is possible to obtain the exact solution of the problem with discontinuous coefficients as well as the regularized problem. These solutions allow us to obtain analytical expressions for the exact error at arbitrary order and to discuss the accuracy of the approximations introduced by the first order expressions obtained previously.

6.1. 1D Laplace equation

The first example considered is the one-dimensional Laplace equation

$$\frac{\partial}{\partial x}\left(D_i \frac{\partial \phi_i}{\partial x}\right) = 0$$

which in the regions of contant diffusivity has as fundamental solution

$$\phi_i = a_i x + b_i. \tag{36}$$

Arbitrarily setting $n = x$, $D_1 = 1$ and $D_2 = D_r$ in a domain $x \in [-1 : 1]$, the analytical solution of the discontinuous problem is

$$\begin{cases} \phi_1 = \frac{D_r(1+x)}{D_r+1} & x \leq 0, \\ \phi_2 = \frac{D_r+x}{D_r+1} & x > 0. \end{cases} \tag{37}$$

The solution of the regularized problem

$$\frac{\partial}{\partial x}\left(\tilde{D} \frac{\partial \tilde{\phi}}{\partial x}\right) = 0$$

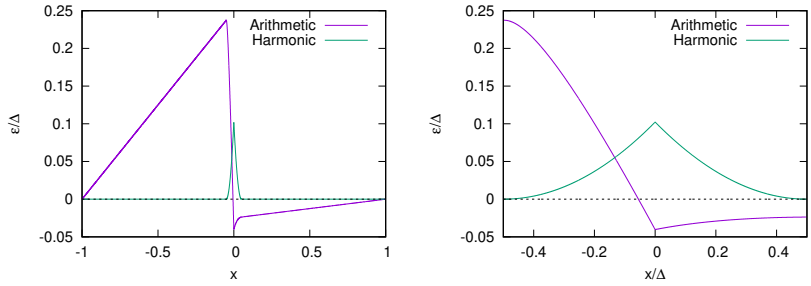

Figure 3: 1D Laplace problem. $D_r = 10$. Comparison of the error field for $\Delta = 1/32$ using the arithmetic mean and the harmonic mean. Left: Error distribution in the entire domain. Right: Error distribution inside the regularization region.

still obeys eq. 36 in the outer regions, while inside the regularized region the solution takes the form

$$\tilde{\phi} = \tilde{c}_1 + \tilde{c}_0 \int \frac{dx}{\tilde{D}}$$

with $\tilde{a}_1, \tilde{a}_2, \tilde{b}_1, \tilde{b}_2, \tilde{c}_0$ and $\tilde{c}_1$ constants to be determined. Setting the boundary conditions at the domain limits and the continuity of $\tilde{\phi}$ and the normal flux across the edges $x = \pm\Delta/2$, we obtain a linear system of six equations that define the constants once a function $\tilde{D}(f)$ is imposed. The exact expressions obtained for the arithmetic and harmonic mean are included in Appendix C. An example of the exact solution of the discontinuous coefficient problem and the regularization problem using the arithmetic mean is shown in figure 2. We clearly see that the solution of the regularized problem converges to that of the discontinuous problem by matching the two linear profiles across the region with diffused interface. Figure 3 compares the structure of the error using the arithmetic and harmonic mean, which is markedly different upon the averaging rule chosen. In this case, the solution is only exact in the bulk regions when the harmonic mean is used as predicted theoretically. From 2(left) we can clearly see that the error in the outer regions is well represented by a linear profile. An approximation at first order is obtained as

$$\epsilon_i' = (a_i - \tilde{a}_i)x + b_i - \tilde{b}_i = -(\tilde{a}_i^{(1)}x + \tilde{b}_i^{(1)})\Delta + \mathcal{O}(\Delta^2).$$

where the values of the coefficients at first order $(\tilde{a}_i^{(1)}, \tilde{b}_i^{(1)})$ can be obtained from the jump conditions of the error and the error flux (eqs. 28-29) and by imposing zero Dirichlet boundary conditions for the error at $x = \pm 1$. The final system of linear equations

$$\begin{cases} [[\epsilon'^{(1)}]] = \tilde{b}_2^{(1)} - \tilde{b}_1^{(1)} = \tilde{J}_{n,0}^{(0)} \left(\frac{\ln(D_r)}{D_r - 1} - \frac{1}{2}\left(1 + \frac{1}{D_r}\right)\right), \\ [[D\frac{\partial \epsilon'^{(1)}}{\partial x}]] = D_r \tilde{a}_2^{(1)} - \tilde{a}_1^{(1)} = 0, \\ \tilde{a}_1^{(1)} - \tilde{b}_1^{(1)} = 0, \\ \tilde{a}_2^{(1)} + \tilde{b}_2^{(1)} = 0, \end{cases} \tag{38}$$

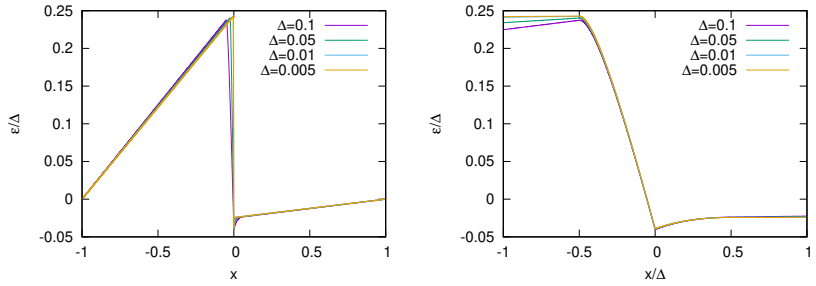

Figure 4: 1D Laplace problem. $D_r = 10$. Arithmetic mean. Spatial structure of the exact error divided by the thickness of the regularization region, ϵ/Δ, for different values of Δ. Left: Error field in the entire domain. Right: Structure of the error inside the regularization region as a function of x/Δ. First order errors dominate the error of the solution. The structure of $\epsilon(x)/\Delta$ outside the regularization region is nearly independent of Δ. The errors inside the regularization region tend to a unique function when represented as a function of x/Δ.

can be solved with the leading order contribution of the normal flux,

$$\tilde{J}^{(0)}_{n,0} = \frac{D_r}{D_r + 1}.$$

The error at $x = \pm\Delta/2$ is given by $b_i^{(1)}$, while the error in the inner regions can be reconstructed using the outer solution and the simplified expressions for the local inner error (eq. 32).

First order errors are present inside the regularized region irrespective of the averaging rule chosen. For the example chosen, the largest errors are found in the case of the arithmetic mean where, unlike the case of the harmonic mean, the error distribution is not symmetric around n=0 (see figure 3). For this particular problem, the error introduced by the arithmetic mean at n=0 is smaller than in the case of the harmonic mean, the difference increasing as the diffusivity difference increases.

Figure 4(left) represents the exact error field obtained with the artihmetic mean for $D_r = 10$. The error is scaled by Δ to clearly see the appearance of a discontinuity as Δ approaches to zero as theoretically predicted by equation 28. The error in the bulk regions is shown to be always first order and its structure in the bulk regions does not depend on the interface thickness, but only on the values of D_r. A parametric study of the the influence of D_r on the error jump predicted with equation 28 and the total error jump between $x = \pm\Delta/2$ shows that the model works well irrespective of the value of D_r chosen (figure 5). Inside the regularized region (figure 4-right), the error profiles obtained for different values of Δ can be represented by a unique function using the dimensionless coordinate x/Δ, which is directly related to f, showing the universality of the structure of the error function inside the regularization region. As theoretically

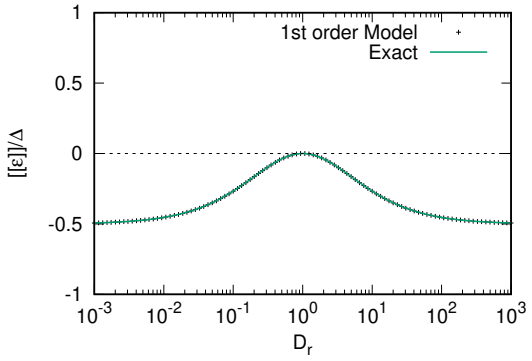

Figure 5: 1D Laplace problem. Comparison between the exact error jump of the outer problem $\frac{[[\epsilon]]}{\Delta}$ and the predicted first order error jump (equation 28) as a function of the diffusivity ratio D_r using the arithmetic for $\Delta = 0.01$.

predicted, the error presents a cusp at n=0 irrespective of the averaging rule used and the error difference between the edge of the regularization region and the error at the center is larger in the region with smallest diffusivity when using the arithmetic mean.

6.2. 1D Poisson equation

We discuss now the numerical errors associated to the solution of the preceeding setup for the case of the Poisson equation with uniform source

$$\frac{\partial}{\partial x}\left(D_i \frac{\partial \phi_i}{\partial x}\right) = 1.$$

We consider homogeneous zero Dirichlet boundary conditions as the influence of any other Dirichlet boundary conditions can be captured by the solution of a decoupled Laplace equation problem. As previously, we arbitrarily set $D_1 = 1$ and $D_2 = D_r$. The general solution of this equation in the bulk regions is

$$\phi_i = \frac{1}{2D_i}x^2 + a_i x + b_i$$

where the solution for the problem with discontinuous coefficients gives

$$a_1 = a_2 D_r = \frac{D_r - 1}{2(1 + D_r)}, \qquad b_1 = b_2 = \frac{-1}{1 + D_r}. \tag{39}$$

For the regularized problem, the fundamental solution in each bulk region must be matched with that inside the interface, where the general solution takes the form

$$\tilde{\phi} = \tilde{c}_1 + \Delta \tilde{c}_0 \int_f^1 \frac{df'}{\tilde{D}} + \Delta^2 \int_f^1 \frac{1 - f'}{\tilde{D}} df', \qquad -\frac{\Delta}{2} \leq x \leq \frac{\Delta}{2}$$

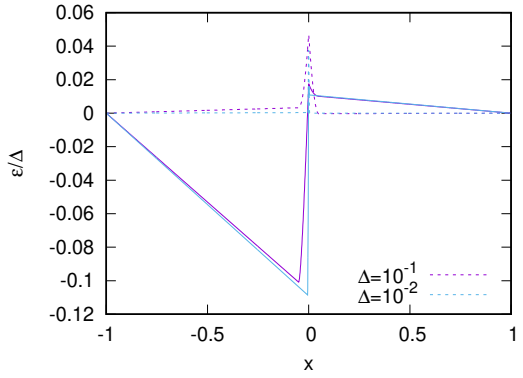

Figure 6: 1D Poisson problem with $D_r = 10$. Total error field for the arithmetic mean (continuous line) and the harmonic mean (dashed line) for two different values of the regularization region thickness.

As before, we obtain a linear system of equations setting the boundary conditions and matching the values of $\tilde{\phi}$ and the flux at $x = \pm\frac{\Delta}{2}$,

$$\begin{bmatrix} -1 & 1 & 0 & 0 & 0 & 0 \\ -\frac{\Delta}{2} & 1 & 0 & -1 & 0 & 0 \\ 1 & 0 & -1 & 0 & 0 & 0 \\ 0 & 0 & -\Delta\int_0^1 \frac{df'}{\tilde{D}} & -1 & \frac{\Delta}{2} & 1 \\ 0 & 0 & -1 & 0 & D_r & 0 \\ 0 & 0 & 0 & 0 & 1 & 1 \end{bmatrix} \begin{bmatrix} \tilde{a}_1 \\ \tilde{b}_1 \\ \tilde{c}_0 \\ \tilde{c}_1 \\ \tilde{a}_2 \\ \tilde{b}_2 \end{bmatrix} = \begin{bmatrix} -0.5 \\ -\Delta^2/8 \\ \Delta/2 \\ \Delta^2\int_0^1 \frac{1-f'}{\tilde{D}}df' - \Delta^2/(8D_r) \\ \Delta/2 \\ -\frac{0.5}{D_r} \end{bmatrix}$$

Figure 6 shows the structure of the exact error for both the arithmentic and the harmonic mean. The error is linear in the bulk regions, scaling with Δ for the case of the arithmetic mean while in the case of the harmonic mean the errors in the outer region converge to zero faster. As previously, the values of the first order errors generated by the arithmetic mean can be obtained from the solution of the system of equations 38 where $J^{(0)}_{n,0} = \frac{D_r-1}{2(D_r+1)}$, while, consistent with theoretical predictions, in the case of the harmonic mean first order errors are zero in the bulk regions

$$\tilde{a}^{(1)}_{1,\text{harm}} = \tilde{b}^{(1)}_{1,\text{harm}} = \tilde{a}^{(1)}_{2,\text{harm}} = \tilde{b}^{(1)}_{2,\text{harm}} = 0.$$

The importance of second order errors can be discussed using equation 24 and subtracting the first order estimation. Using the approximation

$$\tilde{J}^{(0)}_n = J^{(0)}_{n,0} + \left.\frac{\partial \tilde{J}^{(0)}_n}{\partial n}\right|_0 n + \mathcal{O}(n^2).$$

we can conclude that second order errors in the error jump become larger than

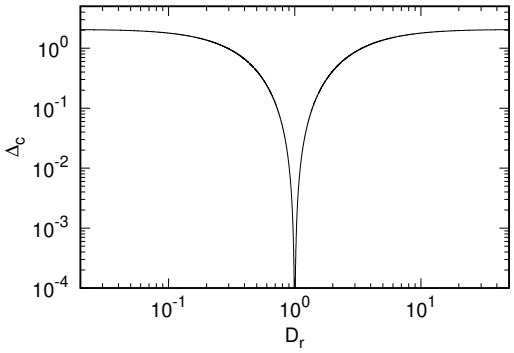

Figure 7: Poisson problem. Theoretical estimation of the critical regularization size Δ_c beyond which second order errors control the solution as a function of D_r

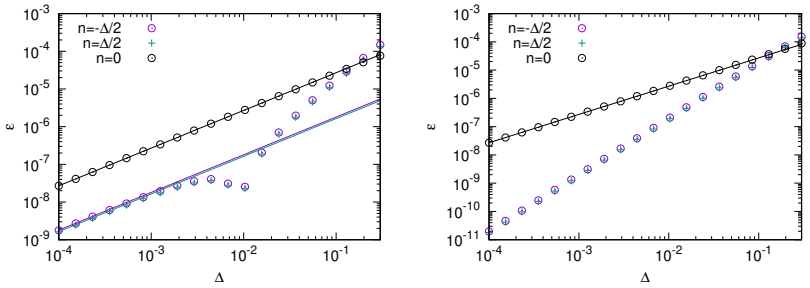

Figure 8: Poisson problem. Convergence curves for the exact error (dots) at $n = -\Delta/2, \Delta/2, 0$ for the artihmetic mean (left) and the harmonic mean (right). $D_r = 1.1$ ($\Delta_c = 0.009$). The solid lines represent the predictions obtained from the solution of the first order model.

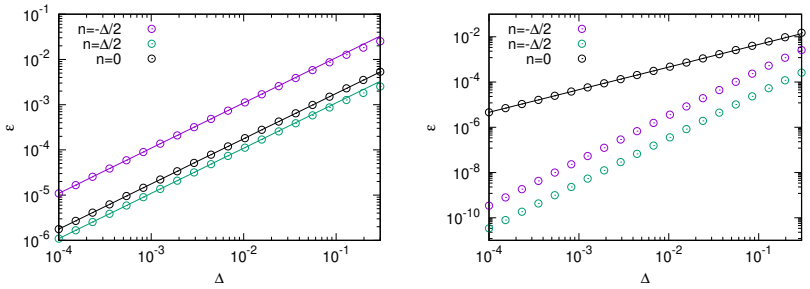

Figure 9: Poisson problem. Convergence curves for the exact error (dots) at $n = -\Delta/2, \Delta/2, 0$ for the artihmetic mean (left) and the harmonic mean (right). $D_r = 10$ ($\Delta_c = 1.78$). The solid lines represent the predictions obtained from the solution of the first order model.

first order errors when

$$|C_1 \tilde{J}^{(0)}_{n,0} \Delta| \ll \left| C_3 \frac{\partial \tilde{J}^{(0)}_n}{\partial n}\bigg|_0 \Delta^2 \right|$$

where C_1 has been defined in eq. 27 and C_3 is a constant that also depends on the averaging rule

$$C_3 \equiv \frac{-[[D]]}{8 D_1 D_2} - \int_0^1 \frac{0.5 - f}{\tilde{D}} df.$$

This unequality can can be rewritten as a condition for Δ as

$$\Delta \gg \Delta_c = \left| \frac{C_1}{C_3} \frac{\tilde{J}^{(0)}_{n,0}}{\frac{\partial \tilde{J}^{(0)}_n}{\partial n}\big|_0} \right|$$

where the normal flux derivative can be expressed as a function of the source using eq. 20 and the ratio C_1/C_3 depends on the average rule chosen and the diffusivity ratio. For this particular problem Δ_c takes small values for values of D_r close to one (see figure 7). The convergence analysis for $D_r = 1.1$ clearly shows that when $\Delta > \Delta_c$ the errors in the bulk regions are controlled by second order errors independently of the choice of the average (figure 8). Only at n=0 first order errors dominate the solution, which are well predicted by the simplified model represented with a black solid line for both the arithmetic mean (equation 33) and the harmonic mean (equation 34). For a sufficiently thin regularization region thickness, $\Delta \ll \Delta_c$, the convergence of the error in the bulk regions in the case of the arithmetic mean is degraded to first order and the first order solution given by the solution of equation 38 works well. For large values of D_r (figure 9), first order errors dominate the solution for all values of the interface thickness using the arithmetic mean, the largest errors found at the edge of the regularization region with the lowest diffusivity (fluid 1). These errors are well captured by the first order model proposed. As in the previous case, the harmonic mean generates second order errors in the bulk regions, first order errors being only visible inside the regularization region and reaching a maximum at n=0 which is well predicted theoretically.

6.3. 2D Laplace equation with a planar interface

We consider now the stationary problem of heat transfer in a 2D rectangular domain $(x, y) \in ([-0.5, 0.5], [0, 1])$ with a discontinuity of the diffusion coefficient D_i at $x = 0$ (e.g. n=x) and the following boundary conditions

$$\phi_2(1/2, y) = f(y), \quad \phi_1(-1/2, y) = 0, \quad \phi_i(x, 0) = 0, \quad \phi_i(x, 1) = 0.$$

We arbitrarily set $D_1 = 1$ and $D_2 = D_r$ where, for the sake of simplicity, we restrict ourselves to cases where $D_r > 1$. In the bulk regions, the general

solution can be obtained using separation of variables: $\phi(x,y) = X(x)Y(y)$. Using the boundary conditions it can be readily shown that the only non-zero solutions correspond to the modes

$$Y_n(y) = \sin(k_n y), \quad k_n = n\pi,$$
$$X_n(x) = a_n e^{n\pi x} + b_n e^{-n\pi x}.$$

The general solution on each side of the box is then a the superposition of the modes $X_n(x)Y_n(x)$

$$\phi_i(x,y) = \sum_{n=1}^{+\infty} \left(a_{n,i} e^{k_n x} + b_{n,i} e^{-k_n x}\right) \sin(k_n y),$$

where the coefficients can be obtained imposing for each mode the boundary conditions on the right and left boundaries and imposing the continuity of fluxes and the field ϕ_i across the interface. This gives the following linear system of equations

$$\begin{bmatrix} e^{-k_n/2} & e^{k_n/2} & 0 & 0 \\ 0 & 0 & e^{k_n/2} & e^{-k_n/2} \\ 1 & 1 & -1 & -1 \\ 1 & -1 & -D_r & D_r \end{bmatrix} \begin{bmatrix} a_{n,1} \\ b_{n,1} \\ a_{n,2} \\ b_{n,2} \end{bmatrix} = \begin{bmatrix} 0 \\ F_n \\ 0 \\ 0 \end{bmatrix}$$

that can be readily solved to find the coefficients $(a_{n,1}, b_{n,1}, a_{n,2}, b_{n,2})$ for each mode from the decomposition of the boundary condition into

$$f(y) = \sum_{n=1}^{\infty} F_n \sin(k_n y).$$

In the following we will restrict ourselves to the discussion of the case $n = 1$ and $F_n = 1$, as this example is sufficient to discuss the structure of the errors generated in a two dimensional problem. Figure 10 shows two examples of the structure of the solution with discontinuous coefficients for $D_r = 1.5$ and $D_r = 10^5$ where we can clearly see how the tangential derivatives at the interface become large as D_r is increased.

When the jump on the coefficients is regularized, the structure of the solution in the regularized region remains to be obtained. In this case the Laplace equation can be written as

$$\frac{\partial \tilde{D}}{\partial x}\frac{\partial \tilde{\phi}}{\partial x} + \tilde{D}\left(\frac{\partial^2 \tilde{\phi}}{\partial x^2} + \frac{\partial^2 \tilde{\phi}}{\partial y}\right) = 0.$$

Using the same separation of variables as before we find:

$$\frac{\partial^2 \tilde{X}}{\partial x^2} + \frac{\partial \tilde{D}}{\partial x}\frac{1}{\tilde{D}}\frac{\partial \tilde{X}}{\partial x} - k_n^2 \tilde{X} = 0, \tag{40}$$

which unlike the expression above involves a damping factor that is dependent on the choice of the regularization function. In a general case, the second

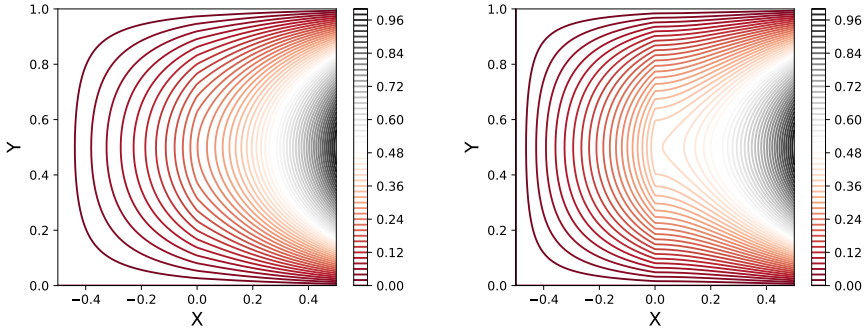

Figure 10: Laplace 2D: Structure of the solution with discontinuous coefficients for $n = 1$ for (left) $D_r = 1.5$ and (right) $D_r = 10^5$.

equation can be rewritten as a Sturm-Liouville problem where the solutions can be obtained from the eigenvalues of the following linear operator:

$$\mathcal{L} = -\frac{1}{\tilde{D}}\frac{\mathrm{d}}{\mathrm{d}x}\left[\tilde{D}\frac{\mathrm{d}}{\mathrm{d}x}\right]$$

Equation 40 can be rewritten as a Bessel ODE in the particular case of the arithmetic mean

$$\zeta^2\frac{\partial^2\tilde{X}}{\partial\zeta^2} + \zeta\frac{\partial\tilde{X}}{\partial\zeta} - \zeta^2\tilde{X} = 0$$

where we have used an additional change of variables

$$\zeta = k_n\Delta\left(\frac{x}{\Delta} + \frac{1+D_r}{2[[D]]}\right) = k_n\Delta\frac{D_1 f + D_2(1-f)}{[[D]]}.$$

This equation admits two eigenvalues, a Bessel's modified function of the first kind I_0 and Bessel's modified function of the second kind K_0. The general solution of the problem in the regularization region can therefore be written as

$$\tilde{\phi}_{\mathrm{arith}}(f) = \sum_{n=1}^{+\infty}\left[\tilde{a}_{n,*}I_0(\zeta) + \tilde{b}_{n,*}K_0(\zeta)\right]\sin(k_n y).$$

Imposing the continuity of ϕ and its flux at the two edges of the diffuse zone and the boundary conditions the coefficients of the solution can be obtained from the solution of the following linear system

$$\begin{bmatrix} e^{-\frac{k_n}{2}} & e^{\frac{k_n}{2}} & 0 & 0 & 0 & 0 \\ 0 & 0 & 0 & 0 & e^{\frac{k_n}{2}} & e^{-\frac{k_n}{2}} \\ -e^{-}_{\Delta} & -e^{+}_{\Delta} & I^{(1)}_{0,\Delta} & K^{(1)}_{0,\Delta} & 0 & 0 \\ -e^{-}_{\Delta} & e^{+}_{\Delta} & I^{(1)}_{1,\Delta} & -K^{(1)}_{1,\Delta} & 0 & 0 \\ 0 & 0 & I^{(2)}_{0,\Delta} & K^{(2)}_{0,\Delta} & -e^{k_n\frac{\Delta}{2}} & -e^{-k_n\frac{\Delta}{2}} \\ 0 & 0 & I^{(2)}_{1,\Delta} & -K^{(2)}_{1,\Delta} & -e^{k_n\frac{\Delta}{2}} & e^{-k_n\frac{\Delta}{2}} \end{bmatrix} \begin{bmatrix} \tilde{a}_{n,1} \\ \tilde{b}_{n,1} \\ \tilde{a}_{n,*} \\ \tilde{b}_{n,*} \\ \tilde{a}_{n,2} \\ \tilde{b}_{n,2} \end{bmatrix} = \begin{bmatrix} 0 \\ 1 \\ 0 \\ 0 \\ 0 \\ 0 \end{bmatrix}$$

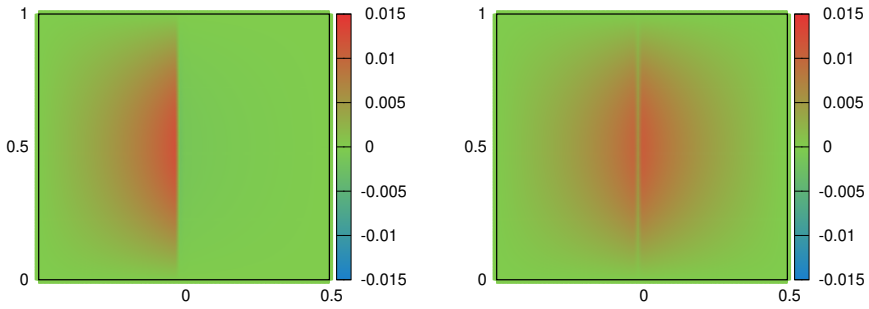

Figure 11: Error fields generated by the solution of the regularized 2D Laplace problem with a flat interface. $D_r = 10$, $\Delta = 10/256$. Left: Arithmetic mean: Right: Harmonic mean.

where we have introduced the following notations for clarity

$$I^{(i)}_{0,\Delta} = I_0\left(k_n\Delta\frac{D_i}{[[D]]}\right), \quad K^{(i)}_{0,\Delta} = K_0\left(k_n\Delta\frac{D_i}{[[D]]}\right),$$
$$I^{(i)}_{1,\Delta} = I'_0\left(k_n\Delta\frac{D_i}{[[D]]}\right), \quad K^{(i)}_{1,\Delta} = -K'_0\left(k_n\Delta\frac{D_i}{[[D]]}\right).$$

For the harmonic mean a similar procedure can be followed to find the solution inside the regularization region

$$\tilde{\phi}_{\text{harm}}(f) = -\sum_{n=1}^{+\infty}\left\{a_{n,*}\chi I_1\left[k_n\chi\right] + b_{n,*}\chi K_1\left[k_n\chi\right]\right\}\sin(k_n y)$$

where

$$\chi = \Delta\frac{D_1(1-f)+D_2 f}{[[D]]}. \tag{41}$$

As previously, the values of the coefficients can be also found by solving the linear system of equations built with the boundary conditions and the matching of the solution and its flux at the edges of the regularization region.

Figure 11 shows an example of the error fields generated by the arithmetic and harmonic mean for $D_r = 10$. The structure of the exact error function along $y = 0.5$ is depicted in figure 12. As theoretically predicted by eqs. 33-34, the error jump in the arithmetic mean tends to be larger in the region of smaller diffusivity while it remains symmetric in the case of the harmonic mean. In this case the errors introduced by the harmonic mean are also first order as a consequence of the two-dimensional nature of the problem. The structure of the error in the regularization region is similar to that reported for the previous problems, where the first order approximation (eqs. 33 and 34) captures remakably well the structure of the error inside the regularization region for different values of Δ (figure 12 right). Figure 13 shows the total error measured with the

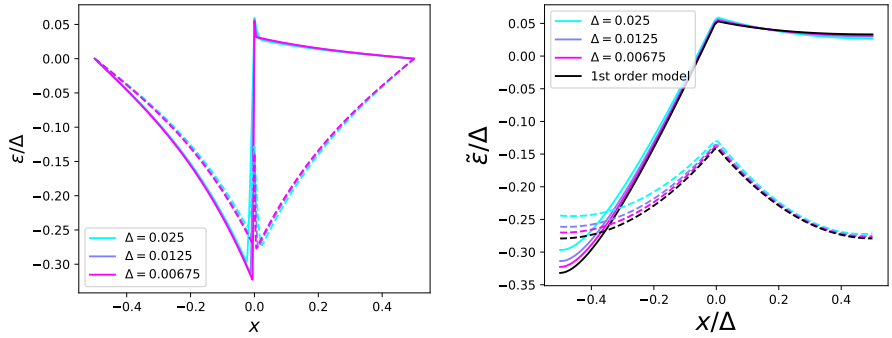

Figure 12: 2D Laplace problem. $D_r = 10$. Left: Spatial structure of the exact error divided by the thickness of the regularization region at $y = 0.5$ obtained with the arithmetic mean (continuous line) and the harmonic mean (dashed line). Right: Zoomed view inside the regularization region. The black line represents the prediction of the structure of the inner error predicted by the first order model.

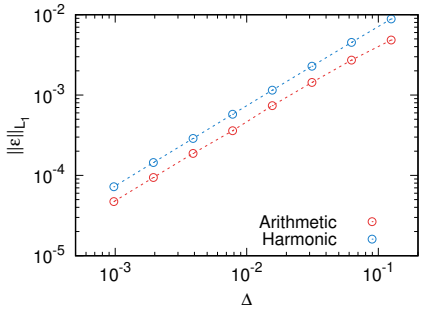

Figure 13: 2D Laplace problem for a flat interface. Convergence rate of the exact analytical error as a function of the thickness of the regularization region (Δ) using the arithmetic mean (red) and harmonic mean(blue). $D_r = 10$.

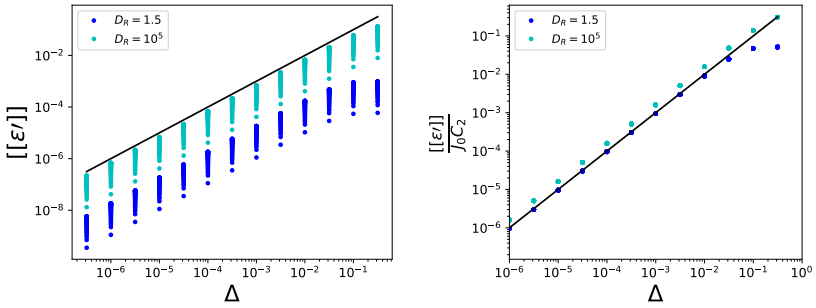

Figure 14: 2D Laplace problem for a flat interface. Arithmetic mean. Left: Exact error jump between $n_1 = -\Delta/2$ and $n_2 = \Delta/2$ obtained analytically for all values of y and different values of the interface thickness Δ for two different values of the diffusivity ratio. Right: Re-scaled error jump using the theoretical prediction for all values of y. With line the predictions of the theoretical model.

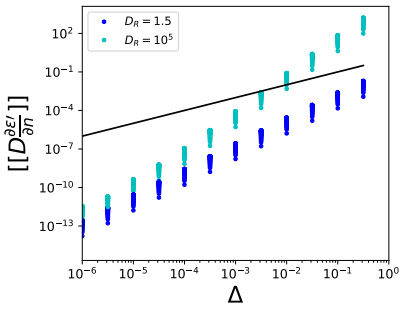

Figure 15: 2D Laplace problem for a flat interface. Arithmetic mean. Exact error flux jump between $n_1 = -\Delta/2$ and $n_2 = \Delta/2$ obtained analytically for all values of y and different values of the interface thickness Δ for two different values of the diffusivity ratio.

L_1 norm as a function of the regularization size thickness. Both the arithmetic and the harmonic mean introduce first order regularization errors in the outer regions. Remarkably in this case the error jump introduced by the arithmetic mean is shown to be beneficial in order to minimize the total error contained in the solution. This example clearly shows that the optimal choice of the regularization function is problem dependent and cannot be concluded that, at least in the continuum limit considered here, there is a universal optimal choice (e.g. we cannot guarantee that the harmonic mean will introduce always less error than the arithmetic mean).

Figure 14(left) depicts the effective error jump across the interface when varying Δ using the arithmetic mean. Different values of y are represented,

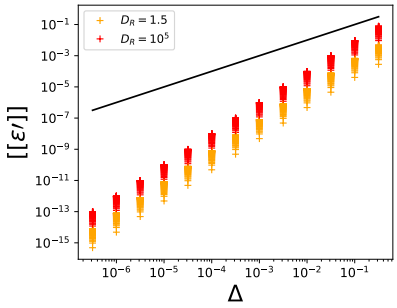

Figure 16: Same results of figure 14 when using the Harmonic mean

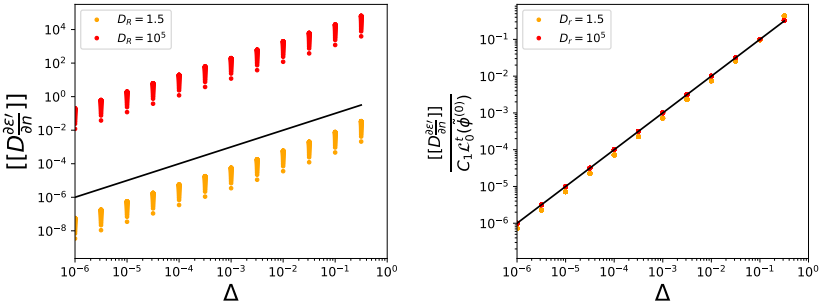

Figure 17: Same results of figure 15 when using the Harmonic mean

both for a small and very large value of the diffusivity. As predicted theoretically, the error jump shows first order convergence. Figure 14right proves that it is possible to collapse all the values of the error jump along y and for the two values of D_r using the first order scaling defined by eq. 26, where the leading order contribution of the normal flux is used and the prefactor C_2 is defined in eq. 27. In addition, figure 15 confirms that the arithmetic mean introduces second order convergence errors in the effective error flux jump condition across an interface of finite size for $D_r = 1.5$ and even third order convergence for $D_r = 10^5$ and sufficiently large values of Δ, this contribution being negligible at first order.

In the case of the harmonic mean (figure 16) second order convergence for the effective error jump condition for the outer problem is displayed. The convergence curves for the error flux jump for all values of y shown in figure 17(left) show that, as expected, the harmonic mean provides first order convergence results for the error flux jump in the outer problem. The first order estimation is well predicted by eq. 25 using the value of the surface Laplacian evaluated at the interface position and the prefactor C_1 defined in eq. 27 (figure 17right).

6.4. 2D Laplace equation with a curved interface

In order to evaluate the influence of the curvature of the interface on the model, we consider now a particular solution of the Laplace problem where an ellipsoid defines an embeded interface. In this case, we can write the Laplacian equation in elliptic-cylinder coordinates as

$$\frac{\partial}{\partial \eta}\left(D\frac{\partial \phi}{\partial \eta}\right) + D\frac{\partial^2 \phi}{\partial \Psi^2} = 0$$

where the change of coordinates is

$$x/a = \cosh(\eta)\cos(\Psi)$$

$$y/a = \sinh(\eta)\sin(\Psi)$$

We set a=1 and define the interface as the isoline of η_I. This value imposes the curvature of the interface which can be parametrized as a function of Ψ as

$$\kappa a = \frac{\sqrt{2}\sinh(2\eta_I)}{(\cosh(2\eta_I) - \cos(2\Psi))^{3/2}}.$$

We look for solutions satisfying the following Dirichlet boundary condition at a distance far from the ellipsoid defined by $\eta = \eta_\infty$,

$$\phi = \cos(\Psi), \qquad \eta = \eta_\infty.$$

As in the preceding example, we restrict ourselves to symmetric solutions where separation of variables exist such that

$$\phi_i = (a_i e^{\eta} + b_i e^{-\eta})\cos(\Psi).$$

The system of equations for the sharp representation of the interface is constructed imposing the boundary conditions and the continuity of ϕ and its normal flux across the interface

$$a_1 = b_1, \tag{42}$$
$$a_2 e^{\eta_\infty} + b_2 e^{-\eta_\infty} = 1, \tag{43}$$
$$a_1 e^{\eta_I} + b_1 e^{-\eta_I} = a_2 e^{\eta_I} + b_2 e^{-\eta_I}, \tag{44}$$
$$D_1(a_1 e^{\eta_I} - b_1 e^{-\eta_I}) = D_2(a_2 e^{\eta_I} - b_2 e^{-\eta_I}). \tag{45}$$

In the regularized problem, we introduce the following regularization function

$$f = 0.5 - \frac{\eta - \eta_I}{\Delta_\eta}$$

where Δ_η is constant. In the physical space, the thickness varies along the interface introducing two characteristic thickness along the y=0 and x=0 axis

$$\Delta_1 = \cosh(\eta_I + 0.5\Delta_\eta) - \cosh(\eta_I - 0.5\Delta_\eta) \approx \sinh(\eta_I)\Delta_\eta$$

$$\Delta_2 = \sinh(\eta_I + 0.5\Delta_\eta) - \sinh(\eta_I - 0.5\Delta_\eta) \approx \cosh(\eta_I)\Delta_\eta$$

which can be expressed in terms of the local value of the curvature as

$$\kappa\Delta_1 = \frac{\Delta_\eta}{\tanh(\eta_I)}, \quad \kappa\Delta_2 = \Delta_\eta \tanh(\eta_I).$$

To find the physical value of the regularization thickness Δ for a given point of the interface (η_I, Ψ_I), we find the distance to this point to the edges of the regularization region defined at $\eta = \eta_I \pm \Delta_\eta/2$ along the normal direction to the interface.

The general solution of the solution inside the regularization region is similar to the one previously found for the 2D Laplace problem for a flat interface. For the arithmetic mean

$$\tilde{\phi}_{\text{arith}}(\eta, \Psi) = \begin{cases} (a_1 e^{\eta} + b_1 e^{-\eta}) \cos(\Psi) & \eta < \eta_I \\ \left(\tilde{a}_* I_0(\zeta) + \tilde{b}_* K_0(\zeta)\right) \cos(\Psi) & \eta_I - \Delta_\eta/2 \leq \eta \leq \eta_I + \Delta_\eta/2 \\ (a_2 e^{\eta} + b_2 e^{-\eta}) \cos(\Psi) & \eta > \eta_I \end{cases}$$

where $\zeta = \frac{\Delta_\eta \tilde{D}(\eta)}{[[D]]}$. The constants in the regularization region are found as before by writing matching conditions at $\eta = \eta_I \pm \Delta_\eta/2$ similarly to the preceeding case for a flat interface.

Figure 18(left) represents the solution obtained for the sharp problem using the arithmetic mean where $D_1 = 1$ (the inner fluid diffusivity) and $D_2 = 10$ (bulk diffusivity). The domain limits are defined by $\eta_\infty = 2$ and the sharp interface position is defined at $\eta_I = 0.1$. The structure of the error introduced by the regularization of the coefficients for $\Delta_\eta = 0.1 \tanh(\eta_I)$ (figure 18right) shows how the error becomes larger in the inner fluid, being the error discontinuous across the interface as in previous cases.

A systematic investigation of the error jump across the diffuse interface in the normal direction for two different values of D_2 and vaying thickness Δ_η is presented in figure 19(left), where in the x-axis we represent the physical thickness Δ for various points lying in the interface (note that the physical value of Δ varies across the interface for a constant value of Δ_η). The results of the error jump introduced between both edges of the regularization region for all the points considered can be collapsed into a single curve using the theoretical model proposed (figure 19right) showing that the curvature does not have a significant influence on the errors generated. Figure 20 depicts the jump on the normal error fluxes across the normal direction in the same locations and values of Δ_η,

$$[[D\frac{\partial \epsilon'}{\partial n}]] = D_2 \frac{\partial \tilde{\epsilon}}{\partial n}\bigg|_{n_2} - D_1 \frac{\partial \tilde{\epsilon}}{\partial n}\bigg|_{n_1}$$

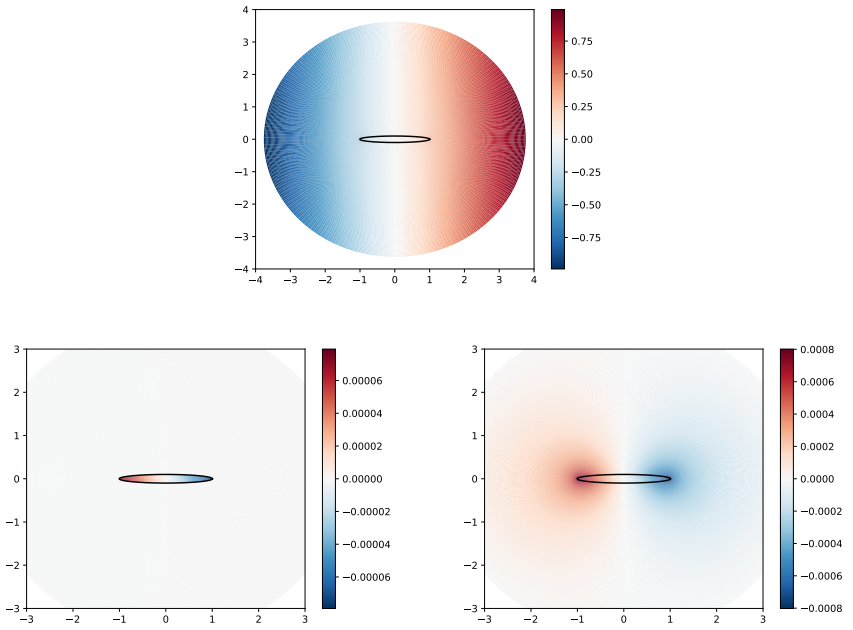

Figure 18: Top: Structure of the solution with discontinuous coefficients for $n = 1$ $a = 1$, $\eta_I = 0.1$ and $D_R = 10$. Bottom: Analytical error map generated by the regularized solution for $\Delta_\eta = 0.1\tanh(\eta_I)$ using (left) the arithmetic mean and (right) the harmonic mean.

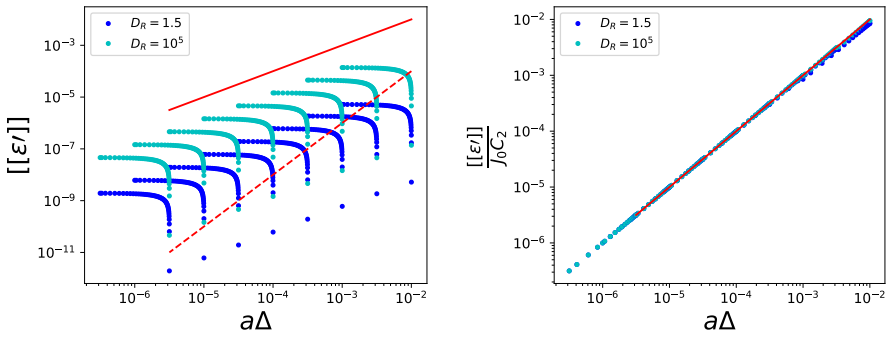

Figure 19: Arithmetic mean. Analytical evaluation of the exact error jump conditions for the outer problem $[[\epsilon]] = \epsilon(\eta_I + \Delta_\eta/2) - \epsilon(\eta_I - \Delta_\eta/2)$ for different values of the interface thickness at different locations of the interface. $\eta_I = 0.1$, $D_1 = 1$ and two different values of $D_2 = 1.5, 10^5$ (Left) Raw data. Red lines showing first and second order convergence are added as reference. (Right) Error jump conditions scaled according to equation 29. The red line denotes the model prediction.

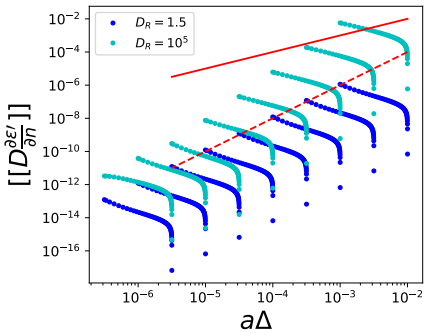

Figure 20: Arithmetic mean. Analytical evaluation of the exact error flux jump conditions for the outer problem $[[D\frac{\partial \epsilon}{\partial n}]]$ for the same conditions of figure 19. Red lines are added as reference to show first and second order convergence rates.

where

$$D_i \frac{\partial \tilde{\epsilon}_i}{\partial n} = \frac{D_i}{\sqrt{\cosh^2(\eta) - \cos^2(\Psi)}} \frac{\partial \tilde{\epsilon}_i}{\partial \eta}.$$

As theoretically predicted, second order convergence is reached.

In the case of the harmonic mean the solution of the system of equations gives

$$\tilde{\phi}_{\text{harm}}(\eta, \Psi) = \begin{cases} (a_1 e^{\eta} + b_1 e^{-\eta}) \cos(\Psi) & \eta < \eta_I \\ -\chi \left(\tilde{a}_* I_1(\chi) + \tilde{b}_* K_1(\chi) \right) \cos(\Psi) & \eta_I - \Delta_\eta/2 \leq \eta \leq \eta_I + \Delta_\eta/2 \\ (a_2 e^{\eta} + b_2 e^{-\eta}) \cos(\Psi) & \eta > \eta_I \end{cases}$$

where χ has been defined in equation 41. Figure 21 shows that the error flux jump condition for the outer problem is proportional to the physical value of the regularization thickness Δ, being possible to collapse all the jump of the effective flux between the edges of the regularization region for all points using the prefactor theoretically computed for flat interfaces and the value of the tangential Laplacian evaluated at the interface. The effective error jump condition (figure 22) is shown to be proportional to Δ^2.

7. Numerical examples

The model presented in this manuscript is formally valid in the continuum limit. For numerical pourposes, this model is expected to be accurate when the grid size h is smaller than the regularization thickness Δ. However, from a practical point of view it is interesting to discuss the behavior of the solution of the discretized Poisson equation for finite values of the dimensionless ratio h/Δ. Note that in the numerical solution regularization errors (if present) are

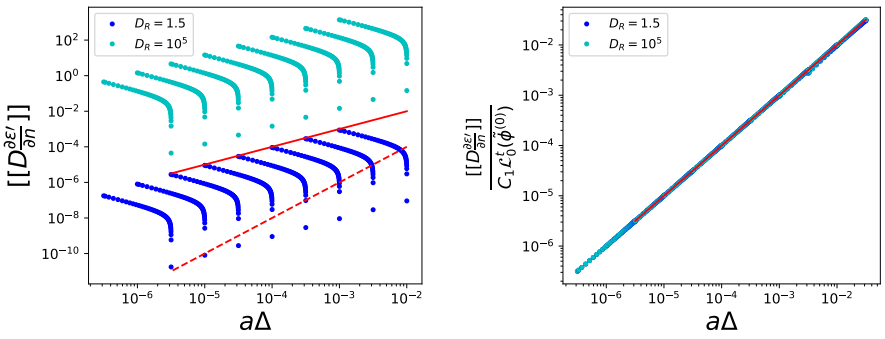

Figure 21: Harmonic mean. Analytical evaluation of the exact normal error flux jump conditions for the outer problem for different values of the interface thickness at different locations of the interface. $\eta_I = 0.1$, $D_1 = 1$ and two different values of $D_2 = 1.5, 10^5$ (Left) Raw data. Red lines showing first and second order convergence are added as reference. (Right) Error jump conditions scaled according to equation 29. The red line denotes the model prediction.

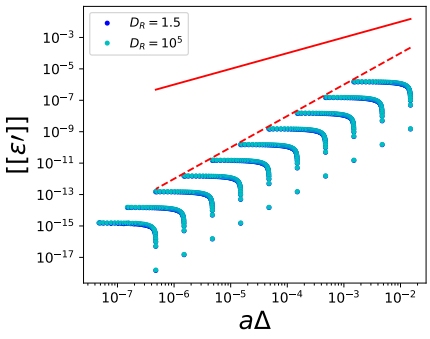

Figure 22: Harmonic mean. Analytical evaluation of the exact error jump condition for the outer problem $[[\epsilon]]$ for the same conditions of figure 22. Red lines are added as reference to show first and second order convergence rates.

not the only source of errors, and discretization errors are certainly present.

In cartesian grids, the discretization of the two-dimensional Poisson equation for the $[i, j]$ cell can be written for both standard second order finite volume discretization and second order finite differences as

$$\tilde{D}_{[i+1/2,j]}\frac{\tilde{\phi}_{[i+1,j]}-\tilde{\phi}_{[i,j]}}{h}-\tilde{D}_{[i-1/2,j]}\frac{\tilde{\phi}_{[i,j]}-\tilde{\phi}_{[i-1,j]}}{h}$$
$$+\tilde{D}_{[i,j+1/2]}\frac{\tilde{\phi}_{[i,j+1]}-\tilde{\phi}_{[i,j]}}{h}-\tilde{D}_{[i,j-1/2]}\frac{\tilde{\phi}_{[i,j]}-\tilde{\phi}_{[i-1,j]}}{h}=\tilde{s}_i h \tag{46}$$

where different choices for the values of the coefficients $\tilde{D}$ can be justified. In this work we will use nodally exact values of $\tilde{D}$ from the definition of f with arbitrary thickness Δ when finite differences will be used. For the VOF method the fraction within a cell is naturally imposed by the initialization method, and it is therefore not straightforward to define a value of Δ independently from h. In this work we consider two different initializations of the regularized coefficients at the cell faces. In the first method the values of f required at the faces will be approximated by the linear interpolation of the void fraction at the cell faces from volume averaged values at the cell center. In addition, we also consider the case where the value of f will be given by the exact fraction of fluid occupying a given cell face. In both cases, the value of Δ cannot be unquestionably defined, although effectively it is expected to be close to the grid size h

In the following, we will use the multigrid solver available in Basilisk [23] to solve the discretized Poisson equation and investigate the numerical errors introduced in problems where the exact solution of the discontinious coefficient problem is available.

7.1. Flat interfaces

In order to gain further insight about the range of validity of the models proposed in numerical applications we use the two-dimensional solution of the Laplace problem considered in section 6.3 to investigate the impact of the discretization on the errors generated in the numerical solution when Δ/h varies. We evaluate $\tilde{D}$ at the desired location from the analytical expression of f given by eq. 3. Because in this problem the interface is flat, the results obtained using finite differences in the limit $\Delta/h = 1$ is similar to the initialization of exact volume average fraction at the cell center from the exact position of the interface and the linear interpolation of it at the faces. Figure 23 shows the results of the L_1 norm of the exact error contained in the numerical solution. The error introduced by the arithmetic mean (figure 23left) is relatively well captured by the model even in the $\Delta = h$ limit, being the quantitative prediction excellent for $\Delta/h \geq 4$. In the case of the harmonic mean (figure 23right) the model captures remarkably well the values of the error for $\Delta/h \geq 2$, but interestingly, the

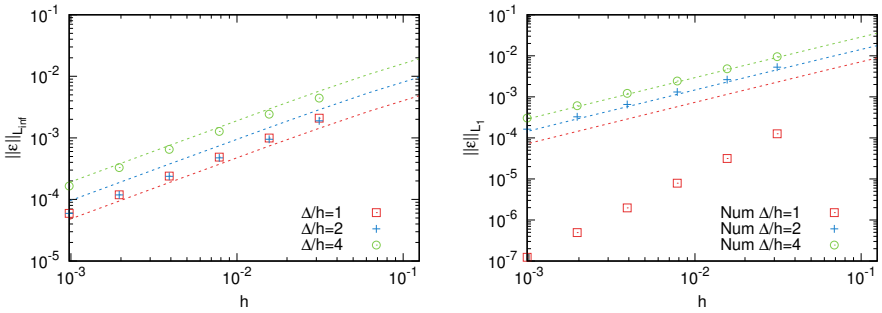

Figure 23: Numerical error generated by the resolution of a 2D Laplace problem for a flat interface. Convergence rate of the numerical error initializing the coefficients with nodally exact values at the face location. Three different ratios of the theoretical regularization length compared to the grid size are tested: $\Delta/h = 1, 2, 4$. Left: Results using the arithmetic mean. Right: Results using the harmonic mean. $D_r = 10$.

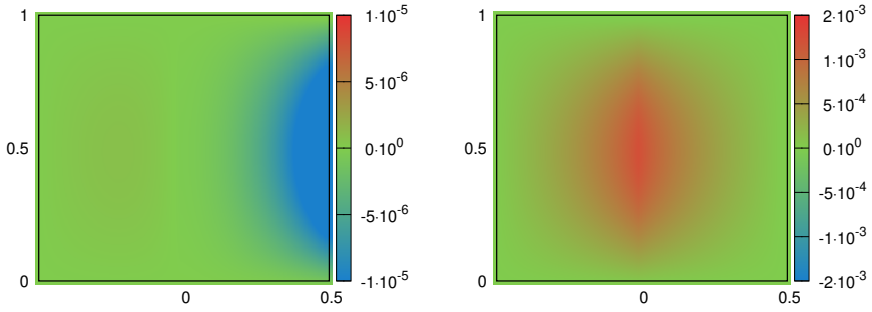

Figure 24: Numerical error generated by the resolution of a 2D Laplace problem for a flat interface. Spatial structure of the exact error using the harmonic mean with (left) $\Delta = h$ and (right) $\Delta = 2h$.

model fails dramatically predicting the errors in the $\Delta = h$ limit, where first order errors vanish and the proposed model is unable to predict the numerical second order convergence observed. To gain further insight into this particular effect, we plot in figure 24 the structure of the error field for a constant value of the grid size $h/L_0 = 1/2^{128}$ and two different values of the thickness of the regularization region: $\Delta = h$ (figure 24 left) and $\Delta = 2h$ (figure 24 right). We clearly see than in the former case the errors are introduced by the boundary condition, the discretization of the interface not showing any significant signature on the error fields obtained. On the contrary, the numerical error fields obtained for $\Delta = 2h$ are consistent with the theoretical prediction obtained in the continuum limit (figure 11 in section 6.3) , being the total numerical errors controlled by the regularization of the coefficients. The fact that it is possible to find discretization schemes able to display second order convergence even in the presence of tangential second order derivatives put in evidence the existence of accurate discretization schemes for sharp interfaces for which the results of this manuscript cannot be applied. However this result must be taken cautiously. Despite the existence of few works attempting to propose second order discretization schemes for multiphase flows [12, 20], generalized second order discretization methods for Eulerian grids where the interface is not aligned with the cell face is an open problem that has not being solved yet [32]. Indeed, as it will be shown next, second order convergence was not observed in numerical problems with curved surfaces using the same combination of the averaging and discretization scheme.

7.2. Curvature effects

In order to investigate the influence of curvature in numerical solutions we solve for two different problems associated to the Poisson equation in an infinite domain where a fluid with diffusivity D_1 and radius R_0 is placed in the bulk of a reference fluid (fluid 2). In polar coordinates, the equation solved can be written as

$$\frac{1}{r}\frac{\partial}{\partial r}(D_i r \frac{\partial \phi_i}{\partial r}) = s,$$

with s a known source. In the first problem considered we impose

$$s = \begin{cases} 1 & r \leq R_0, \\ 0 & r > R_0, \end{cases}$$

and boundary conditions

$$\left.\frac{\partial \phi_1}{\partial r}\right|_{r=0} = 0, \qquad \phi_1(r=0) = 0.$$

The general solution for this problem in the sharp limit is

$$\phi = \begin{cases} \frac{sR_0^2 (r/R_0)^2}{4D_1}, & r \leq R_0, \\ \frac{sR_0^2}{2D_2}\ln(r/R_0) + \frac{sR_0^2}{4D_1}, & r > R_0. \end{cases}$$

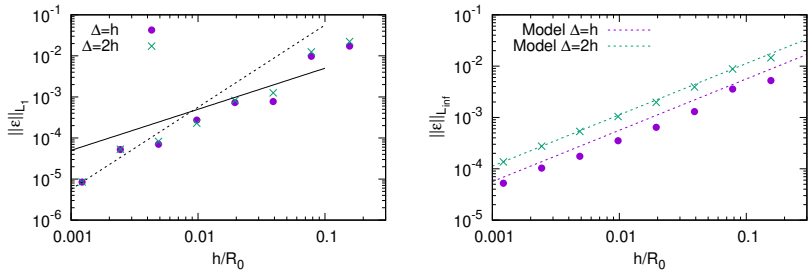

Figure 25: Convergence study for the solution of the Poisson equation for $D_2/D_1 = 10$ using nodally exact face values, the harmonic mean, and two different values of the ratio Δ/h. (Left) L_1 norm. Two reference lines for first and second convergence are added as reference. (Right) L_∞ norm, the dashed lines represent the solution of the first order model.

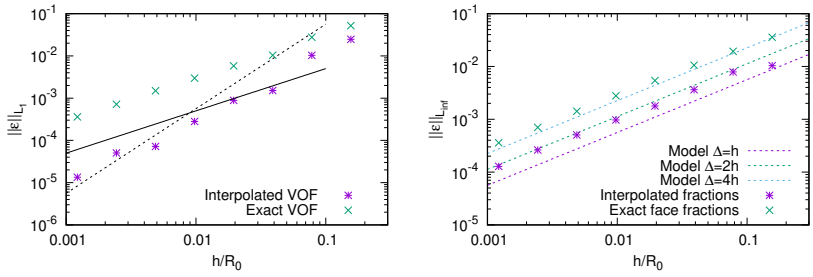

Figure 26: Convergence study for the solution of the Poisson equation for $D_2/D_1 = 10$ using the harmonic mean for two different values of the ratio Δ/h and using the VOF method using the interpolated values of the fraction at the cell faces (symbol *) and using the exact face fraction values ($\times$). (left) L_1 norm. Two reference lines for first and second convergence are added as reference. (Right) L_∞ norm, the dashed lines we represent the solution of the first order model in the continuum limit.

Numerically, we solve for the discretized Poisson equation in a cartesian grid with uniform grid size h in a square domain of size $L_0 = 5$, where exact Dirichlet boundary conditions are imposed. We set $R_0 = 1$, $D_1 = 1$ and $D_2 = 10$. We start investigating the dependence of the numerical errors with the grid size for the harmonic mean using nodally exact values of the face fraction (finite differences) and imposing the value of the ratio Δ/h (figure 25). Nearly second order convergence is observed for the errors measured in the L_1 norm, where the errors do not depend on Δ, while the convergence is degraded to first order in the L_∞ norm. This observation is consistent with the predictions of the theoretical models, where the harmonic mean is supossed to introduce second order effective jump conditions for the outer error, being first order errors only visible inside the regularization region. Although the errors in the L_1 norm cannot be obtained analytically for the particular simulation conditions used, the L_∞ first order error can still be predicted theoretically from eq. 34 where the outer error is imposed to be zero. In general, the model proposed predicts remarkably well the maximum first order errors when nodally exact face values of f are used to define $\tilde{D}$ using the harmonic mean even in the case $h = \Delta$, where we previously found second order convergence in the case of a flat interface.

Figure 26 shows the errors introduced by the definition of exact face averaged fractions as well as interpolated fractions from cell centered averaged fractions (finite volume approach). The use of interpolated values is shown to provide comparable results to nodally exact values for $\Delta = h$ for the second order errors measured in the L_1 norm. Remarkably, L_∞ errors are larger than in the case of finite differences, being close to the model predictions for $\Delta = 2h$. The errors measured in both L_1 and L_∞ norm are reduced when using face interpolated values from cell centered values of the VOF function than exact face averaged value obtained from the exact position of the interface, where the errors are close to the model predictions for $\Delta = 4h$. Note that indeed the definition of mixed face fractions in a given cell modifies the solution in a 3×3 stencil, so it is not surprising to find that classical implementations of VOF effectively introduce regularization errors with larger effective values of Δ than h. We therefore conclude that at least in standards implementations of the volume of fluid method the curvature of the interface is sufficient to introduce regularization errors that are well predicted by the theory.

To conclude, we discuss also the errors of the numerical solution for a modified problem where the source contains an azimuthal component

$$s = \begin{cases} \frac{3}{4} D_1 R_0^2 \cos(\theta), & r \leq R_0, \\ -\left(\frac{D_2}{2} + D_1 \ln(r/R_0)\right) \frac{R_0^4}{2r^2} \cos(\theta), & r > R_0. \end{cases} \tag{47}$$

The exact solution of this problem for a sharp interface is

$$\begin{cases} \phi_1 = \frac{D_1 r^2}{4} \cos(\theta), & r \leq R_0, \\ \phi_2 = \left(\frac{1}{4} + \frac{\ln(r/R_0)}{2D_2}\right) D_1 R_0^2 \cos(\theta), & r > R_0. \end{cases} \tag{48}$$

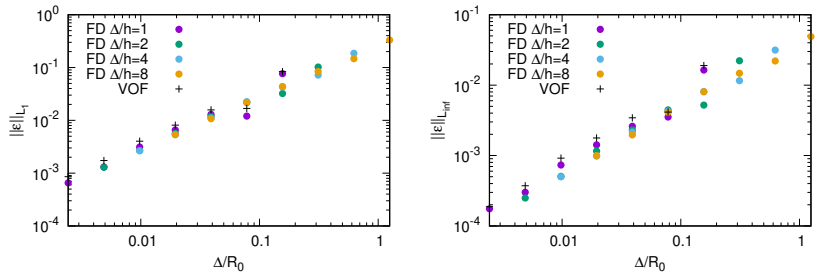

Figure 27: Convergence test for the solution of the Poisson equation obtained with the harmonic mean. The source is given in eq. 47. Results are obtained using Finite Differences (FD) with different values of the Δ/h ratio (dots) and using face interpolated values of the cell averaged fraction (VOF).

The main difference with the previous case is the presence of a tangential component, effectively introducing first order errors in the outer solution even with the use of an harmonic mean. Using the same parameters than the previous case to obtain the numerical solution, the grid size is varied between $h = L_0/2^5$ and $L_0/2^{11}$. Figure 27 shows the results obtained using the harmonic mean and a finite difference discretization, where the values of the diffusion coefficient at the cell faces are initialized with the nodally exact value of the regularization function with a given value of the ratio Δ/h. In addition the results obtained with the standard VOF method are included, where the values at the cell faces are computed from the interpolation of the fluid fraction defined at the cell center. Due to the presence of tangential gradients both, the L_1 and the L_∞ norm display first order convergence, with the preactor of the errors introduced by the various methods scaling with Δ and not h. As in the previous example, for a given value of h, the most accurate results are obtained imposing $\Delta = h$ and using nodally exact values of the fraction f on the cell faces.

8. Conclusions and perspectives

This manuscript presents a systematic approach to investigate the errors introduced by the regularization of the jump of the coefficients in the solution of an elliptic equation. Using a multiscale analysis the error is decomposed into an inner region associated to a small length scale Δ and an outer region. The error in the outer region is shown to obey a Laplace equation with jump conditions accross the interface on the error and the error flux. The analysis of the inner problem allows obtaining expressions for the effective jump conditions required in the outer problem at arbitrary order and expressions for the structure of the error in the inner region.

The theoretical analysis reveals that the first order approximation of the error jump required for the resolution of the outer problem is proportional to

the normal flux of the regularized solution across the interface, while the first order approximation of the error flux source depends on the value of the surface Laplacian of the regularized solution evaluated at a given point of the interface. In both cases, exact expressions for the pre-factors depending on the averaging rule are given. In the particular case of the arithmetic mean, the regularization of the interface only introduces an error flux source in the outer problem at first order, being the error jump always null. In the case of the harmonic mean, the effective error jump vanishes, only generating first order errors in the outer solution in multidimensional problems. Remakably, the inner error is shown to be always first order and proportional to the normal flux of the regularized solution irrespective of the averaging rule used.

Various analytical examples where it is possible to compute exact expressions of the regularization error are used to provide convincing evidence about the relevance of the first order error estimations in the approximate solution. In addition, numerical tests show that except in some particular cases the error model proposed captures the main source of numerical errors even in situations where the grid size becomes of the order of the regularization length Δ, providing an accurate representation of the error distribution in the entire domain.

Future extensions of this work include the discussion of regularization models to account for the presence of discontinuities on the primitive variable and its flux as well as the generalization to more complex equations or system of equations.

Appendix A. Transient effects

In many cases the one-fluid formulation is applied for transients problems introducing additional complexity on the analyses of the errors introduced. As an extension of the results shown for steady-state problems let's consider as an example the transient diffusion-reaction equation

$$a_i(x)\frac{\partial \phi_i}{\partial t} = \nabla \cdot (D_i \nabla \phi_i) - s_i, \tag{A.1}$$

where $a_i(x)$ and $D_i(x)$ are spatial functions that do not depend on time. The classical form of the regularized problem is written as

$$\tilde{a}(x)\frac{\partial \tilde{\phi}}{\partial t} = \nabla \cdot (\tilde{D} \nabla \tilde{\phi}) - \tilde{s}. \tag{A.2}$$

Following a similar manipulation than in the steady problem we find that the problem for the error evolution in the entire domain obeys

$$a_i \frac{\partial \epsilon_i}{\partial t} = \nabla \cdot (D_i \nabla \epsilon_i) - S_{\epsilon_i} - (a_i - \tilde{a})\frac{\partial \tilde{\phi}}{\partial t}, \tag{A.3}$$

with the same expressions for the source (eq. 5) and the jump conditions (eqs. 6-7) derived for steady problems. Imposing that the last term in the right hand

size is not null only inside the regularized region, then the outer problem reduces to an unsteady diffusion equation for the outer error

$$a_i \frac{\partial \epsilon_i'}{\partial t} = \nabla \cdot (D_i \nabla \epsilon_i'). \tag{A.4}$$

Following the same procedure explained in the core of the manuscript we can readily integrate the equations in the normal direction to find the jump conditions at first order

$$[[D \frac{\partial \epsilon_f'^{(1)}}{\partial n}]] = C_1 \mathcal{L}_0^t(\tilde{\phi}^{(0)}) + \frac{\partial \tilde{\phi}^{(0)}}{\partial t}\bigg|_{n=0} \frac{1}{\Delta} \int_{n_1}^{n_2} (a_i - \tilde{a}) dn \tag{A.5}$$

$$[[\epsilon_f'^{(1)}]] = C_2 \tilde{J}_{n,0}^{(0)}, \tag{A.6}$$

with the integration constants given by eqs. 27-27. We can see that compared to the steady-state solution, transient effects introduces an additional source of error appears in the error flux jump when the function a_i is regularized. Remarkably, it can be easily checked that at first order the structure of the inner error remains unchanged with respect to the steady state problem.

Appendix B. Local coordinate system for the inner problem

Appendix B.1. Local coordinate system for two-dimensional surfaces

To integrate the error equation along the normal direction in the two dimensional case, we use polar coordinates

$$\xi_n = r, \quad \xi_{t_1} = \theta, \quad \xi_{t_2} = z$$

to define a local coordinate system where the local value of the curvature of the interface at $\boldsymbol{x}_I$ imposes (see figure 1)

$$r = \frac{1}{\kappa_1} - n.$$

The scale factors are

$$h_{\xi_n} = 1, \quad h_{\xi_{t_1}} = r, \quad h_{\xi_{t_2}} = 1$$

such that

$$\mathcal{K} = \frac{1}{h_{\xi_n} h_{\xi_{t_1}} h_{\xi_{t_2}}} \frac{\partial (h_{\xi_{t_1}} h_{\xi_{t_2}})}{\partial \xi_n} = \frac{1}{r} = \frac{\kappa_1}{1 - \kappa_1 n} \approx \kappa_1 + \mathcal{O}(\Delta \kappa_1^2).$$

Appendix B.2. Local coordinate system for three-dimensional surfaces

In three dimensions we use an oblate spheroidal coordinate system

$$\xi_n = \eta, \quad \xi_{t_1} = \theta, \quad \xi_{t_2} = \psi.$$

to represent the actual interface by an iso-surface placed at $\eta = \eta_I$. The two principal curvatures at $(\eta, \theta, \psi) = (\eta_I, 0, \pi/2)$, κ_1 and κ_2, define the parameters a and η_I as:

$$\kappa_2 = \frac{1}{a\ \sinh(\eta_I)}, \qquad \kappa_1 = \frac{\tanh(\eta_I)}{a\ \cosh(\eta_I)}$$

where κ_2 is the value of the principal with the largest absolute value.

Using the definitions of the metric factors [16],

$$h_{\xi_n} = a\sqrt{\cosh^2(\eta) - \sin^2(\theta)}, \quad h_{\xi_{t_1}} = a\sqrt{\cosh^2(\eta) - \sin^2(\theta)}, \quad h_{\xi_{t_2}} = a\cosh(\eta)\sin(\theta)$$

we readily obtain

$$\mathcal{K} = \frac{1}{h_{\xi_n} h_{\xi_{t_1}} h_{\xi_{t_2}}} \frac{\partial \left(h_{\xi_{t_1}} h_{\xi_{t_2}} \right)}{\partial \xi_n} = \frac{2\sinh(\eta)}{a\cosh^2(\eta)} = 2\kappa_1 + \mathcal{O}(\Delta)$$

Appendix C. Exact solution of the regularized 1D Laplace problem

The solution of the 1D regularized problem of section 6.1 can be expressed as

$$\tilde{\phi} = \begin{cases} \tilde{a}_1 x + \tilde{b}_1 & x < -\Delta/2, \\ \tilde{c}_1 + \tilde{c}_0 \int \frac{dx}{\tilde{D}} & -\Delta/2 \le x\ \le \Delta/2, \\ \tilde{a}_2 x + \tilde{b}_2 & x > \Delta/2. \end{cases} \tag{C.1}$$

For the arithmetic mean, the solution obtained after imposing the boundary conditions and matching conditions across the interface gives

$$\begin{aligned} \tilde{a}_{1,\text{arith}} &= \tilde{a}_{2,\text{arith}} D_r = \tilde{b}_{1,\text{arith}} = \tilde{c}_{1,\text{arith}} = \frac{D_r}{D_r + 1 - \left(\frac{1+D_r}{2} - D_r \frac{\ln(D_r)}{D_r - 1} \right) \Delta}, \\ \tilde{b}_{2,\text{arith}} &= \frac{D_r - (\frac{1+D_r}{2} - D_r \frac{\ln(D_r)}{D_r - 1})\Delta}{D_r + 1 - \left(\frac{1+D_r}{2} - D_r \frac{\ln(D_r)}{D_r - 1} \right) \Delta}, \\ \tilde{c}_0 &= 1 - \frac{\Delta}{2}. \end{aligned}$$

while for the harmonic mean the result is

$$\begin{aligned} &\tilde{a}_{1,\text{harm}} = \tilde{a}_{2,\text{harm}} D_r = \tilde{b}_{1,\text{harm}} = \tilde{b}_{2,\text{harm}} = \tilde{c}_{0,\text{harm}} = \frac{D_r}{D_r + 1}, \\ &\tilde{c}_{1,\text{harm}} = \frac{D_r + \frac{1}{8}\Delta(1 - D_r)}{D_r + 1}. \end{aligned} \tag{C.2}$$

References

[1] Alauzet, F., Loseille, A., 2016. A decade of progress on anisotropic mesh adaptation for computational fluid dynamics. Computer-Aided Design 72, 13–39. URL: https://www.sciencedirect.com/science/article/pii/S0010448515001517, doi:https://doi.org/10.1016/j.cad.2015.09.005.

[2] Allaire, G., Brizzi, R., 2005. A multiscale finite element method for numerical homogenization. Multiscale Modeling & Simulation 4, 790–812.

[3] Anderson, D.M., McFadden, G.B., Wheeler, A.A., 1998. Diffuse-interface methods in fluid mechanics. Annual review of fluid mechanics 30, 139–165.

[4] Aniszewski, W., Arrufat, T., Crialesi-Esposito, M., Dabiri, S., Fuster, D., Ling, Y., Lu, J., Malan, L., Pal, S., Scardovelli, R., et al., 2019. Parallel, robust, interface simulator (paris) .

[5] Babuška, I., 1976. Solution of interface problems by homogenization. i. SIAM Journal on Mathematical Analysis 7, 603–634.

[6] Baer, M.R., Nunziato, J.W., 1986. A two-phase mixture theory for the deflagration-to-detonation transition (ddt) in reactive granular materials. International journal of multiphase flow 12, 861–889.

[7] Belme, A., Dervieux, A., Alauzet, F., 2012. Time accurate anisotropic goal-oriented mesh adaptation for unsteady flows. Journal of Computational Physics 231, 6323–6348. URL: https://www.sciencedirect.com/science/article/pii/S0021999112002276, doi:https://doi.org/10.1016/j.jcp.2012.05.003.

[8] Drew, D.A., 1983. Mathematical modeling of two-phase flow. Annual review of fluid mechanics 15, 261–291.

[9] Fuster, D., Colonius, T., 2011. Modelling bubble clusters in compressible liquids. Journal of Fluid Mechanics 688, 352–389.

[10] Fuster, D., Popinet, S., 2018. An all-mach method for the simulation of bubble dynamics problems in the presence of surface tension. Journal of Computational Physics 374, 752–768.

[11] Kadioglu, S.Y., Nourgaliev, R.R., Mousseau, V.A., 2008. A comparative study of the harmonic and arithmetic averaging of diffusion coefficients for non-linear heat conduction problems. Technical Report. Idaho National Lab.(INL), Idaho Falls, ID (United States).

[12] LeVeque, R.J., Li, Z., 1994. The immersed interface method for elliptic equations with discontinuous coefficients and singular sources. SIAM Journal on Numerical Analysis 31, 1019–1044.

[13] Loseille, A., 2008. Adaptation de maillage anisotrope 3D multi-échelles et ciblée à une fonctionnelle pour la mécanique des fluides : Application à la prédiction haute-fidélité du bang sonique. Thèse de doctorat. Paris 6. URL: http://www.theses.fr/2008PA066622.

[14] Maddix, D.C., Sampaio, L., Gerritsen, M., 2018. Numerical artifacts in the generalized porous medium equation: Why harmonic averaging itself is not to blame. Journal of Computational Physics 361, 280–298.

[15] Marigo, J.J., Maurel, A., Pham, K., Sbitti, A., 2017. Effective dynamic properties of a row of elastic inclusions: the case of scalar shear waves. Journal of elasticity 128, 265–289.

[16] Moon, P., Spencer, D.E., 2012. Field theory handbook: including coordinate systems, differential equations and their solutions. Springer.

[17] Nevard, J., Keller, J.B., 1997. Homogenization of rough boundaries and interfaces. SIAM Journal on Applied Mathematics 57, 1660–1686.

[18] Papanicolau, G., Bensoussan, A., Lions, J.L., 1978. Asymptotic analysis for periodic structures. Elsevier.

[19] Patankar, S.V., 1978. A numerical method for conduction in composite materials, flow in irregular geometries and conjugate heat transfer, in: International Heat Transfer Conference Digital Library, Begel House Inc.

[20] Peskin, C.S., 2002. The immersed boundary method. Acta numerica 11, 479–517.

[21] Pham, K., Mercier, J.F., Fuster, D., Marigo, J.J., Maurel, A., 2021. Scattering of acoustic waves by a nonlinear resonant bubbly screen. Journal of Fluid Mechanics 906, A19.

[22] Popinet, S., 2009. An accurate adaptive solver for surface-tension-driven interfacial flows. Journal of Computational Physics 228, 5838–5866.

[23] Popinet, S., 2015. A quadtree-adaptive multigrid solver for the serre–green–naghdi equations. Journal of Computational Physics 302, 336–358.

[24] Prosperetti, A., Tryggvason, G., 2009. Computational methods for multiphase flow. Cambridge university press.

[25] Saade, Y., Lohse, D., Fuster, D., 2023. A multigrid solver for the coupled pressure-temperature equations in an all-mach solver with vof. Journal of Computational Physics 476, 111865.

[26] Scardovelli, R., Zaleski, S., 1999. Direct numerical simulation of free-surface and interfacial flow. Annual review of fluid mechanics 31, 567–603.

[27] Schmidmayer, K., Bryngelson, S.H., Colonius, T., 2020a. An assessment of multicomponent flow models and interface capturing schemes for spherical bubble dynamics. Journal of Computational Physics 402, 109080.

[28] Schmidmayer, K., Petitpas, F., Le Martelot, S., Daniel, É., 2020b. Ecogen: An open-source tool for multiphase, compressible, multiphysics flows. Computer Physics Communications 251, 107093.

[29] Schneider, M., 2021. A review of nonlinear fft-based computational homogenization methods. Acta Mechanica 232, 2051–2100.

[30] Sussman, M., Smereka, P., Osher, S., 1994. A level set approach for computing solutions to incompressible two-phase flow. Journal of Computational physics 114, 146–159.

[31] Tomar, G., Gerlach, D., Biswas, G., Alleborn, N., Sharma, A., Durst, F., Welch, S.W., Delgado, A., 2007. Two-phase electrohydrodynamic simulations using a volume-of-fluid approach. Journal of Computational Physics 227, 1267–1285.

[32] Tryggvason, G., Scardovelli, R., Zaleski, S., 2011. Direct numerical simulations of gas–liquid multiphase flows. Cambridge University Press.

[33] Wackers, J., Deng, G., Guilmineau, E., Leroyer, A., Queutey, P., Visonneau, M., Palmieri, A., Liverani, A., 2017. Can adaptive grid refinement produce grid-independent solutions for incompressible flows? Journal of Computational Physics 344, 364–380. URL: https://www.sciencedirect.com/science/article/pii/S0021999117303650, doi:https://doi.org/10.1016/j.jcp.2017.04.077.

[34] Wang, B., Cleary, M., Masri, A., 2021. Modeling of interfacial flows based on an explicit volume diffusion concept. Physics of Fluids 33.

[35] Xiao, F., Honma, Y., Kono, T., 2005. A simple algebraic interface capturing scheme using hyperbolic tangent function. International journal for numerical methods in fluids 48, 1023–1040.

[36] Xiao, F., Ii, S., Chen, C., 2011. Revisit to the thinc scheme: a simple algebraic vof algorithm. Journal of Computational Physics 230, 7086–7092.

[37] Zhikov, V.V., Kozlov, S.M., Oleinik, O.A., Ngoan, K.T., 1979. Averaging and g-convergence of differential operators. Russian Mathematical Surveys 34, 69.